

Retrieving Heterogeneous Surface Soil Moisture at 100 m across the Globe via Synergistic Fusion of Remote Sensing and Land Surface Parameters

Jingyi Huang¹, Ankur Rashmikanth Desai², Jun Zhu², Alfred E Hartemink¹, Paul Stoy³, Steven P Loheide II², Yakun Zhang², Zhou Zhang², and Francisco J. Arriaga²

¹UNIVERSITY OF WISCONSIN-MADISON

²University of Wisconsin-Madison

³University of Wisconsin - Madison

November 23, 2022

Abstract

Soil water is essential for maintaining global food security and for understanding hydrological, meteorological, and ecosystem processes under climate change. Successful monitoring and forecasting of soil water dynamics at high spatio-temporal resolutions globally are hampered by the heterogeneity of soil hydraulic properties in space and complex interactions between water and the environmental variables that control it. Current soil water monitoring schemes via station networks are sparsely distributed while remote sensing satellite soil moisture maps have a very coarse spatial resolution. In this study, an empirical surface soil moisture (SSM) model was established via data fusion of remote sensing (Sentinel-1 and Soil Moisture Active and Passive Mission - SMAP) and land surface parameters (e.g. soil texture, terrain) using a quantile random forest (QRF) algorithm. The model had a spatial resolution of 100 m and performed moderately well across the globe under cropland, grassland, savanna, barren, and forest soils ($R = 0.53$, $RMSE = 0.08$ m m). SSM was retrieved and mapped at 100 m every 6-12 days in selected irrigated cropland and rainfed grassland in the OZNET network, Australia. It was concluded that the high-resolution SSM maps can be used to monitor soil water content at the field scale for irrigation management. The SSM model is an additive and adaptable model, which can be further improved by including soil moisture network measurements at the field scale. Further research is required to improve the temporal resolution of the model and map soil water content within the root zone.

Hosted file

globalwatermodel_tables_02052020.docx available at <https://authorea.com/users/529106/articles/601322-retrieving-heterogeneous-surface-soil-moisture-at-100-m-across-the-globe-via-synergistic-fusion-of-remote-sensing-and-land-surface-parameters>

1 **Retrieving Heterogeneous Surface Soil Moisture at 100 m across the Globe via Synergistic**
2 **Fusion of Remote Sensing and Land Surface Parameters**

3

4 Jingyi Huang^{1,*}, Ankur R. Desai², Jun Zhu³, Alfred E. Hartemink¹, Paul C. Stoy⁴, Steven P.
5 Loheide II⁵, Yakun Zhang¹, Zhou Zhang⁴, Francisco Arriaga¹

6

7 ¹Department of Soil Science, University of Wisconsin-Madison, Madison, WI 53706, USA

8 ²Department of Atmospheric and Oceanic Sciences, University of Wisconsin-Madison, Madison,
9 WI 53706, USA

10 ³Department of Statistics and Entomology, University of Wisconsin-Madison, Madison, WI
11 53706, USA

12 ⁴Department of Biological Systems Engineering, University of Wisconsin-Madison, Madison,
13 WI 53706, USA

14 ⁵Department of Civil & Environmental Engineering, University of Wisconsin, Madison, WI
15 53706, USA

16

17

18 E-mail: jhuang426@wisc.edu

19

20 * – Corresponding author

21

22 *Keywords:* soil moisture network; machine learning; food security; drought; gross primary
23 productivity; evapotranspiration; water use efficiency;

24 **Abstract**

25 Soil water is essential for maintaining global food security and for understanding hydrological,
26 meteorological, and ecosystem processes under climate change. Successful monitoring and
27 forecasting of soil water dynamics at high spatio-temporal resolutions globally are hampered by
28 the heterogeneity of soil hydraulic properties in space and complex interactions between water
29 and the environmental variables that control it. Current soil water monitoring schemes via *in situ*
30 station networks are sparsely distributed while remote sensing satellite soil moisture maps have a
31 very coarse spatial resolution. In this study, an empirical surface soil moisture (SSM) model was
32 established via data fusion of remote sensing (Sentinel-1 and Soil Moisture Active and Passive
33 Mission - SMAP) and land surface parameters (e.g. soil texture, terrain) using a quantile random
34 forest (QRF) algorithm. The model had a spatial resolution of 100 m and performed moderately
35 well across the globe under cropland, grassland, savanna, barren, and forest soils ($R^2 = 0.53$,
36 $RMSE = 0.08 \text{ m}^3 \text{ m}^{-3}$). SSM was retrieved and mapped at 100 m every 6-12 days in selected
37 irrigated cropland and rainfed grassland in the OZNET network, Australia. It was concluded that
38 the high-resolution SSM maps can be used to monitor soil water content at the field scale for
39 irrigation management. The SSM model is an additive and adaptable model, which can be further
40 improved by including soil moisture network measurements at the field scale. Further research is
41 required to improve the temporal resolution of the model and map soil water content within the
42 root zone.

43 **1. Introduction**

44 Water plays a fundamental role in terrestrial ecosystems and human society. Soil water is a
45 critical factor for a number of terrestrial biochemical, climate, and atmospheric processes and is
46 the source of water for most of the crops that we eat (Vereecken et al., 2014). Monitoring and
47 forecasting soil water content and fluxes (e.g. evapotranspiration, deep drainage) are essential for
48 maintaining global food security (Hoekstra and Mekonnen, 2012) and understanding
49 hydrological, meteorological, and ecosystem processes under climate change (Seneviratne et al.,
50 2010; Trugman et al., 2018; Stoy et al., 2019).

51 Successful monitoring and forecasting soil water content and fluxes at high spatio-
52 temporal resolutions globally is hampered by many factors, including heterogeneity of soil
53 hydraulic properties in space (Robinson et al., 2008), complex interactions between water,
54 environment, and human activities (Vereecken et al., 2014), and computational challenges
55 (Chaney et al., 2018). Current regional and continental soil water monitoring networks are too
56 sparsely distributed (e.g. ~100 km) to be used for field-scale research and application (e.g.
57 irrigation) while remote sensing satellite soil moisture missions often have a coarse spatial
58 resolution (> 1 km) (Ochsner et al., 2017).

59 Recent technological advances provide a potential solution to mapping soil water
60 variability at the field scale. First, high-resolution remote sensing satellite missions have been
61 launched to monitor soil water dynamics and land surface parameters (e.g. vegetation, terrain,
62 and soil properties) have become available (Reuter et al., 2007; Friedl et al., 2010; Hengl et al.,
63 2017; Fisher et al., 2017), which characterize the heterogeneity of land cover, soil, and terrain
64 features at the field scale. Second, machine learning and supercomputers have been increasingly
65 used to model complex interactions between water content and fluxes with environmental
66 variables (Lu et al., 2015 and 2017; Adeyemi et al., 2018; Chaney et al., 2018; Prasad et al.,
67 2018). Therefore, it is possible to combine these remote sensing and land surface datasets for
68 improved delineation of soil water variability at the field scale.

69 Though earlier attempts have made successes on mapping surface soil moisture (SSM) at
70 finer resolutions (i.e. 500 m to 1 km) using empirical and mechanistic models with European
71 Space Agency Sentinel-1 (ESA-Sentinel-1) and/or National Aeronautics and Space
72 Administration - Soil Moisture Active Passive (NASA-SMAP) Mission data with different
73 spatial and temporal resolutions (Lievens et al., 2017; Bauer-Marschallinger et al., 2018; Das et

74 al., 2019; Guevara and Vargas, 2019; Reichle et al., 2019), one unresolved research question
75 remains: how much further can we improve the spatial and temporal resolutions of the models to
76 characterize the heterogeneity of SSM at scales relevant for management of food and water
77 resources?

78 To answer the question, this paper will focus on two objectives: 1) to develop an empirical
79 machine learning model that is able to retrieve and map SSM across the globe at 100-m every 6-
80 12 days over 4 years (2016–2019) by synergistic fusion of remote sensing data from Sentinel-1
81 and SMAP with land surface parameters via a machine learning algorithm (quantile random
82 forest); 2) to apply the SSM model to selected irrigated cropland and rainfed grassland in the
83 semi-arid region of Australia to demonstrate the potential application of the high-resolution
84 machine learning based SSM maps for irrigation management. Our working hypothesis is a
85 combination of remote sensing and land surface parameters data will improve the model
86 performance of SSM retrieval at the field scale (i.e. 100 m).

87

88 **2. Materials and Methods**

89 2.1. Remote Sensing and Land Surface Data

90 Ground SSM measurements from various soil moisture networks were used as training and
91 validation data for the remote sensing and land surface data that were used as covariates to
92 retrieve SSM across the globe. Both remote sensing and land surface datasets were spatially
93 explicit with the remote sensing data time-varying and the land surface datasets time-constant
94 (Figure 2 and Table 1).

95

Table 1 (near here)

96 2.2. NASA SMAP Mission

97 The SMAP mission was launched by the NASA, which provides land surface measurements
98 across the globe with a revisit time of 2-3 days. It relies on the simultaneous measurements of L-
99 band backscatter from an active synthetic-aperture radar (SAR) and brightness temperature from
100 a passive L-band radiometer to retrieve SSM (Lievens et al., 2017). The sensors operate at a
101 constant incidence angle. The use of L-band microwave signals enables detection of land surface
102 moisture under moderate vegetation cover, through cloud cover, and during day and night. Since
103 the failure of the radar in 2015, the SMAP mission can only retrieve SSM based on the passive
104 radiometer. In this study, the SMAP_L3_SM_P product was used, which retrieves SSM at 0–

105 0.05 m with a resampled spatial resolution of $36 \text{ km} \times 36 \text{ km}$ and a revisit time of 2-3 days
106 across the globe based on a physical model using the brightness temperature and other ancillary
107 datasets (O'Neill et al., 2015).

108 SMAP data were downloaded from Earth Data (<https://earthdata.nasa.gov/>) using the R
109 platform (Version 3.6.0) with the package “smapr” (Version 0.2.1) from March 1st to October 1st
110 between 2016 and 2019. The period was selected to avoid frozen soils within the various soil
111 moisture networks because of the poor performance of SSM retrieval over frozen ground.
112 Afterward, the data were gap-filled pixel-wise using a simple temporal moving average with a
113 window size of 3 days using the “imputeTS” package. The small window size was selected to
114 avoid smoothing of SSM due to its strong variability over time. This generated SSM estimates at
115 a $36 \text{ km} \times 36 \text{ km}$ resolution on a daily basis during the study period, which were used as time-
116 varying covariates for modeling SSM.

117

118 2.3. ESA Sentinel-1 mission

119 Sentinel-1 mission was launched by the European Space Agency (ESA), which consists of C-
120 band SARs situated at a two-satellite constellation operating at dual polarizations: single co-
121 polarization with vertical transmit/vertical receive (abbreviated as VV) and dual-band cross-
122 polarization with vertical transmit/horizontal receive (abbreviated as VH). It measures the land
123 surface backscatter intensity at VV and VH polarizations with a varying incidence angle with a
124 spatial resolution of $5 \text{ m} \times 20 \text{ m}$ and a revisit time of 6–12 days. The use of a C-band microwave
125 signal leads to a reduced penetration depth of Sentinel-1’s sensors under moderate vegetation
126 cover compared to SMAP. The relationship between SAR backscatter and the dielectric constant
127 of the soil (a function of soil moisture) enables retrieval of SSM from the Sentinel-1 data.
128 Because the empirical model of the Sentinel-1 mission only retrieves relative SSM instead of soil
129 volumetric water content (Bauer-Marschallinger et al., 2018), and because the physical retrieval
130 model is currently under development (Lievens et al., 2017), the backscatter and incidence angle
131 data were selected as covariates. Here, classical physical models (e.g. Oh et al., 1992; Fung,
132 1994; Dubois et al., 1995) were not used to retrieve SSM from the Sentinel-1 data because
133 researchers have reported poor performance of the physical models when SSM is large and land
134 surface roughness is high (Merzouki et al., 2011; Lievens et al., 2017).

135 The backscatter data were preprocessed using the Sentinel-1 Toolbox
136 (<https://sentinel.esa.int/web/sentinel/toolboxes/sentinel-1>) within the Google Earth Engine
137 platform (<https://developers.google.com/earth-engine/sentinel1>), which involves thermal noise
138 removal, radiometric calibration, and terrain correction using Shuttle Radar Topography Mission
139 (SRTM) 30-m digital elevation model (Rabus et al., 2003). To minimize the speckle effects of
140 the resampled Sentinel-1 radar data (Gao et al., 2017), additional preprocessing procedures were
141 applied using the Google Earth Engine platform (Gorelick et al., 2017). This was suggested by
142 Bauer-Marschallinger et al. (2018) and involved dynamic masking the extreme backscatter
143 values outside the normal ranges for VV (−5 to −25 dB) and VH (−10 to −30 dB), spatial
144 aggregating to 100 m × 100 m, and filtering with a 3 × 3 Gaussian filter. The processed Sentinel-
145 1 data included backscatter data and incidence angle values at a 100 m × 100 m resolution with a
146 revisit time of 6–12 days, which were used as time-varying covariates for modeling SSM.

147 To facilitate the retrieving of SSM from Sentinel-1 data, a number of temporal indices
148 were calculated from the processed Sentinel-1 backscatter images pixel-wise to account for the
149 land surface characteristics, such as temporal minimum, mean, maximum, and standard deviation
150 (SD) of the backscatter data. These temporal statistics of the sensor measurements over time
151 contain characteristics of the soil and vegetation in the field (Huang et al., 2019) and were used
152 as time-constant covariates for modeling SSM.

153

154 2.4. Terrain Parameters

155 In addition to remote sensing datasets that can be directly used to retrieve SSM, terrain
156 parameters that characterize topography characteristics have been used to indirectly model or
157 downscale SSM (Entekhabi et al., 2010; Guevara and Vargas, 2019). In this study, a 500-m
158 aggregated version of the Digital Elevation Model (DEM) from the Global Multi-resolution
159 Terrain Elevation Data 2010 (GMTED2010) was used to calculate a number of primary and
160 secondary terrain parameters (Olaya, 2009), including slope, aspect, terrain position index (TPI),
161 and terrain ruggedness index (TRI) using the “terrain” function from the R package “raster”
162 (Hijmans et al., 2015). Because SMAP SSM data had a coarser resolution (36 km), a finer-
163 resolution (e.g. 30–250 m) DEM was not used. Elevation data were not used for SSM modeling
164 process because of the insufficient long-term SSM stations at high elevation across the world

165 (e.g. Tibetan Plateau). In addition, topographic wetness index was not calculated because it was
166 strongly correlated to TPI at the 500-m resolution.

167

168 2.5. Soil Properties

169 Soil physical and chemical properties affect soil water retention and redistribution in space and
170 time (Mohanty and Skaggs, 2001). Although finer-resolution maps of soil properties are
171 available in many countries where the soil moisture networks are installed (e.g. Grundy et al.,
172 2015; Ramcharan et al., 2018; Chaney et al., 2019), a consistent global map of soil properties
173 was preferred for SSM modeling. In this study, 250-m resolution maps of soil properties were
174 used, which include clay and sand content, bulk density (BD), soil organic carbon content from
175 the SoilGrids (Hengl et al., 2017), and newly mapped field capacity and permanent wilting point
176 (Hengl and Gupta, 2019).

177

178 2.6. Land Cover

179 Land surface characteristics vary with different LC types and had different impacts on the spatial
180 and temporal variations of SSM and the performance of SSM models (Entekhabi et al., 2010). To
181 facilitate the interpretation of the SSM models, 500-m annual land cover (LC) data were
182 downloaded during 2016 from the MODIS repository (MCD12Q1.006, available at
183 <https://lpdaac.usgs.gov/products/mcd12q1v006/>). The International Geosphere-Biosphere
184 Programme (IGBP) classification was used, among which were six merged LC types were
185 selected, including cropland, grassland, savanna, shrubland, forest, and barren. These LC types
186 were not used as covariates for retrieving SSM (due to the coarse resolution) but were used to
187 evaluate the performance of the SSM models under different LC types.

188

189 2.7. Soil Moisture Monitoring Networks

190 Soil moisture networks have been established across the world to provide long-term
191 climate reference measurements for meteorological monitoring, hydrological modeling, and
192 validating of remote sensing products (Dorigo et al., 2011; Quiring et al., 2016). Here, two types
193 of soil moisture networks were used: regional-scale and continental-scale networks (Figure 1). A
194 summary of the number of stations used in this study is provided in Table 2. Details about the
195 site characterization of these networks can be found in the references mentioned above.

196
197
198
199
200
201
202
203
204
205
206
207
208
209
210
211
212
213
214
215
216
217
218
219
220
221
222
223
224
225

Table 2 (near here)

Regional-scale soil moisture networks consist of the Murrumbidgee soil moisture monitoring networks of the OZNET in New South Wales, Australia (Smith et al., 2012), Soil Moisture Measurement Stations Network of the University of Salamanca, Spain (REMEDIUS) (Martínez-Fernández and Ceballos, 2005), and the Danish hydrological observatory (HOBE) in Denmark (Jensen and Illangasekare, 2011). These networks were selected because they were located at the regional scale ($< 50,000 \text{ km}^2$) and can be used to characterize variations of surface soil moisture within catchments, and span a variety of soil moisture and climatic regimes each with significant spatial variability. It was expected that soil moisture measurements from these regional-scale networks can provide detailed information for retrieving SSM within the coarse pixels of the SMAP SSM product (36 km).

Continental-scale soil moisture networks consist of National Oceanic and Atmospheric Administration sponsored US Climate Reference Network (USCRN, Janis and Center, 2002) and the United States Department of Agriculture Natural Resources Conservation Service soil climate analysis network (SCAN, Schaefer et al., 2007). These networks are sparsely situated across the USA with several stations within each state, but they cover a variety of climate regimes, terrain parameters, land cover types, and soil texture classes. It was expected that the use of these widely spread networks can provide information on the relationship between climate regimes, terrain parameters, land cover types, and soil texture classes with SSM and improve the robustness of the SSM model.

2.8. Establishing Empirical SSM Retrieval Models

Random Forest is a nonparametric model based on similarities among observations to fit decision trees. To determine a split at a node in a tree, a random subsample of predictor variables is taken to select the predictor that minimizes the regression error. Nodes continue to be split until no further improvement in error is achieved. The prediction is achieved with an adaptive neighborhood classification and regression. Omitted observations, termed the “out-of-bag” sample, are used to compute the regression errors for trees (Breiman, 2001; Hastie et al., 2009). To estimate the quantiles of the predictions, the Quantile Random Forest (QRF) algorithm was applied using the R ‘quantregForest’ package (Version 1.3-7, Meinshausen and Meinshausen,

226 2017), which estimates the conditional distribution based on a weighted distribution of observed
227 model response values (Meinshausen, 2006).

228 To train the QRF model and evaluate the model performance, SSM measurements from
229 the various soil moisture networks were randomly split into training and validation datasets. To
230 maximally represent the heterogeneous land surface conditions and variations of SSM, 75% of
231 the measuring stations from the regional-scale (OZNET, REMEDHUS, HOBE) and continental-
232 scale (USCRN, SCAN) networks were randomly selected as the training dataset and the
233 remaining 25% of the stations from these four networks were used as the validation dataset
234 (Figure 1). The coefficient of determination (R^2), mean error (bias), and root mean squared error
235 (accuracy) were calculated for both calibration and validation datasets using the measured SSM
236 at the stations and predicted SSM from the QRF models. The 5% and 95% quantiles of the
237 predictions were also calculated to present the confidence of the SSM prediction.

238 **Fig. 1–2 (near here)**

239
240 2.9. Prediction of SSM on an Irrigated Farm in Australia

241 SSM was predicted at the field scale in Australia during the 2018 growing season. The flowchart
242 of the algorithm is presented in Figure 2. The study area was located in the Yanco site of the
243 OZNET, New South Wales, Australia. The annual precipitation was approximately 402 mm with
244 annual minimum and maximum temperatures of 11.5 and 24.2 °C. Furrow irrigation is often used
245 over the growing season every one to two weeks. SSM was retrieved and mapped using the
246 established QRF model across a number of irrigated fields and rainfed (totally 13,822 ha in size)
247 on selected days during the early season from November to December 2018. This period was
248 selected due to a reported drought in the region (BBC, 2018; BOM, 2018).

249 To demonstrate the usefulness of the high-resolution QRF model and evaluate the
250 impacts of water stress on plant productivity, MODIS satellite-based 500-m 8-day cumulative
251 gross primary productivity (GPP, g C m^{-2} per 8 days, <https://lpdaac.usgs.gov/products/mod17a2hv006/>) and evapotranspiration (ET, $\text{mm H}_2\text{O}$ per 8
252 days, <https://lpdaac.usgs.gov/products/mod16a2v006/>) were downloaded across the study fields.
253 The 8-day cumulative GPP and ET data were temporally interpolated with the centers of the 8-
254 day periods matched with the dates of the SSM maps. Water use efficiency was calculated across
255 the fields as the ratio of GPP to ET ($\text{g Carbon per mm H}_2\text{O}$).
256

257

258 3. Results

259 3.1. Model Performance of the QRF and SMAP Product

260 The importance of the variables is presented in Figure 3. SMAP was ranked as the most
261 important time-varying variables, followed by Sentinel-1 backscatter data measured at VV and
262 VH polarizations, and incidence angle of the Sentinel-1. In terms of the time-constant variables,
263 sand content was most important, followed by the temporal mean of VH backscatter data,
264 topographic ruggedness index, topographic position index, aspect, clay content, and other
265 variables.

266 The model performance of the fitted QRF model is also presented in Figure 3. The model
267 has an RMSE of $0.02 \text{ m}^3 \text{ m}^{-3}$ and R^2 of 0.95 for the training dataset and a reduced performance
268 with an RMSE of $0.08 \text{ m}^3 \text{ m}^{-3}$ and R^2 of 0.53 for the validation dataset. The SSM estimates from
269 SMAP had an overall similar performance (no significant difference) for the same validation
270 dataset with an RMSE of $0.08 \text{ m}^3 \text{ m}^{-3}$ and R^2 of 0.50.

271 **Table 3 and Fig. 3–4 (near here)**

272

273 3.2. Model Performance of the QRF and SMAP Product within Different Land Cover Types

274 Pearson's correlation coefficient (r), mean error (ME), and root mean squared error
275 (RMSE) calculated between measured SSM from the station soil moisture networks and
276 predicted SSM from the QRF model or SMAP were used to evaluate the model performance
277 within different land cover types. When all networks were considered (Table 3), the empirical
278 QRF model established via combination of SMAP, Sentinel-1 and land surface parameters
279 outperformed the SMAP SSM estimates for cropland ($r = 0.73$ vs. 0.64 , RMSE = 0.08 vs. 0.10
280 $\text{m}^3 \text{ m}^{-3}$) and savanna ($r = 0.73$ vs. 0.54 , RMSE = 0.09 vs. $0.11 \text{ m}^3 \text{ m}^{-3}$). Both QRF and SMAP
281 models had similar performance under barren ($r = 0.77$ vs. 0.77 , RMSE = 0.05 vs. $0.06 \text{ m}^3 \text{ m}^{-3}$)
282 and forest ($r = 0.58$ vs. 0.63 , RMSE = 0.09 vs. $0.08 \text{ m}^3 \text{ m}^{-3}$) soils. However, the QRF model was
283 worse than the SMAP in grassland ($r = 0.63$ vs. 0.67 , RMSE = 0.07 vs. $0.07 \text{ m}^3 \text{ m}^{-3}$) and
284 shrubland soils ($r = 0.22$ vs. 0.63 , RMSE = 0.07 vs. $0.05 \text{ m}^3 \text{ m}^{-3}$).

285 Similar patterns were observed for each network within different land cover types (Table
286 3) and for the temporal dynamics of measured and estimated SSM at several selected validation
287 stations (Figure 4). It was evident that the QRF model was more accurate than SMAP under

288 cropland (OZNET – Uri_Park, $r = 0.81$ vs. 0.79 , RMSE = 0.06 vs. $0.14 \text{ m}^3 \text{ m}^{-3}$) and Savanna
289 (HOBE – 3.06, $r = 0.55$ vs. 0.56 , RMSE = 0.06 vs. $0.12 \text{ m}^3 \text{ m}^{-3}$), similar to SMAP under barren
290 (SCAN – Lovelock NNR, $r = 0.70$ vs. 0.67 , RMSE = 0.05 vs. $0.06 \text{ m}^3 \text{ m}^{-3}$) and forest (SCAN –
291 Reynolds Homestead, $r = 0.60$ vs. 0.57 , RMSE = 0.08 vs. $0.15 \text{ m}^3 \text{ m}^{-3}$), and worse than SMAP
292 under grassland (REMEDHUS – Las_Arenas, $r = 0.82$ vs. 0.79 , RMSE = 0.09 vs. $0.07 \text{ m}^3 \text{ m}^{-3}$)
293 and shrubland (USCRN – CA_Fallbrook_5_NE, $r = 0.05$ vs. 0.04).

294 It should also be noted that large variations of model performance (i.e. Pearson's r , ME,
295 RMSE) were observed for all land cover types among different ground SSM stations, indicating
296 strong heterogeneity of land surface parameters at the field scale. In summary, we note that the
297 QRF model was able to successfully retrieve SSM dynamics under cropland ($r = 0.73$, RMSE =
298 $0.08 \text{ m}^3 \text{ m}^{-3}$), grassland ($r = 0.63$, RMSE = $0.07 \text{ m}^3 \text{ m}^{-3}$), savanna ($r = 0.73$, RMSE = $0.09 \text{ m}^3 \text{ m}^{-3}$)
299 3), forest ($r = 0.58$, RMSE = $0.09 \text{ m}^3 \text{ m}^{-3}$), and barren ($r = 0.77$, RMSE = $0.05 \text{ m}^3 \text{ m}^{-3}$) soils.

300

301 3.3. Delineating SSM Variations at the Field scale via Data Fusion

302 Coarse-resolution SMAP SSM maps can not be used to reveal spatial SSM variations at the field
303 scale compared to the data fusion based QRF model (Figure 5). In the selected fields within the
304 OZNET network in Australia, SSM was retrieved and mapped using the QRF from November
305 9th to December 15th, 2018. During this early cropping season, SSM varied greatly over time
306 (0.06 – $0.18 \text{ m}^3 \text{ m}^{-3}$). Instead of showing uniform values for the whole region at different days
307 from the 36-km SMAP model (0.19 , 0.14 , 0.07 , and $0.18 \text{ m}^3 \text{ m}^{-3}$), the mean SSM values of the
308 QRF maps displayed strong heterogeneity in space with ranges of SSM of 0.06 , 0.12 , and 0.06
309 $\text{m}^3 \text{ m}^{-3}$ under the dry (December 3rd), intermediate (transitional) (November 21st, December 15th),
310 and wet (November 9th) conditions, respectively.

311 MODIS-estimated 8-day cumulative GPP and ET also displayed strong variations in
312 space and over the study period (15 – 27 g C m^{-2} per 8 days and 400 – $1,200 \text{ mm H}_2\text{O}$ per 8 days)
313 (Figure 5). Note that GPP and ET values were higher in the northern parts of the region
314 associated with the irrigated crops and lower in the southern parts of the region associated with
315 the rainfed grassland.

316 Three sites were selected across the region, including two irrigated cropland fields (1 and
317 2) and one rainfed grassland. As shown in Figures 5 and 7, irrigated cropland 1 had a higher
318 SSM on November 9th ($0.18 \text{ m}^3 \text{ m}^{-3}$) and other days than irrigated cropland 2 ($0.17 \text{ m}^3 \text{ m}^{-3}$) and

319 rainfed grassland ($0.15 \text{ m}^3 \text{ m}^{-3}$). This was consistent with the higher GPP and ET values
320 observed (e.g. November 9th) for irrigated cropland 1 (41 g C m^{-2} per 8 days and $1,760 \text{ mm H}_2\text{O}$
321 per 8 days), cropland 2 (27 g C m^{-2} per 8 days and $1,000 \text{ mm H}_2\text{O}$ per 8 days) and rainfed
322 grassland (16 g C m^{-2} per 8 days and $670 \text{ mm H}_2\text{O}$ per 8 days). Also note that different water use
323 efficiency values were observed between the two irrigated cropland sites and the rainfed
324 grassland.

325

326

Fig. 5–7 (near here)

327

328 **4. Discussion**

329 4.1. Model Performance under Different Land Cover Types

330 In terms of the model performance, the empirical data fusion based SSM model is superior or
331 similar to the 36-km SMAP_L3 SSM product under many land cover types except for grassland
332 and shrubland. Improved model accuracy under cropland and savanna is most likely due to the
333 use of high-resolution (5–20 m) Sentinel-1 data compared to SMAP (~ 36 km), which
334 characterize field-scale variations in SSM (Figures 5–7). However, due to the use of a C-band
335 microwave signal, it is expected that the Sentinel-1’s radar has a reduced penetration depth as
336 compared to the L-band SMAP passive microwave radiometer under moderate to dense
337 vegetation cover conditions (Lievens et al., 2017). This helps explain the poor performance of
338 the SSM model under shrubland. In terms of grassland, the slightly worse performance of the
339 SSM model can also be due to the grazing or harvesting practices that change the vegetation
340 characteristics (e.g. leaf area).

341

342 4.2. A tradeoff between Spatial and Temporal Resolutions of Remote Sensing Soil Moisture 343 Products

344 Current remote sensing soil moisture missions operating at the global scale are based on
345 reflectance in the optical band (e.g. MODIS), passive microwave (e.g. SMOS, SMAP, SMAR2,
346 ASCAT), active microwave (e.g. Sentinel-1, RADARSAT-2) and gravity (GRACE). As shown
347 in Figure 8 and summarized by others (Robinson et al., 2008; Vereecken et al., 2014; Wang et
348 al., 2009; Ochsner et al., 2013), there is a tradeoff between the spatial and temporal resolutions
349 of these satellites. In general, optical and active microwave satellites have a fine spatial

350 resolution less than 1 km but the temporal resolution (revisit time) is more than one week. By
351 contrast, passive microwave satellites have a coarse spatial resolution larger than 10 km but the
352 temporal resolution is higher (1-3 days). The gravity-based mission (GRACE) measures soil
353 water in the deep profile, and has a large spatial resolution (> 100 km) with a temporal resolution
354 of approximately one month.

355 The SSM model established here has a spatial resolution of 100 m and revisit time of 6-
356 12 days (depending on the location of the study sites) across the globe. Many researchers have
357 attempted to retrieve SSM at a similar (100 m) or higher (30 m) spatial resolution using Sentinel-
358 1 data at the field scale using a larger number of ground-based SSM measurements (e.g.
359 Alexakis et al., 2017; Gao et al., 2017; Attarzadeh et al., 2018). However, the model
360 performance deteriorates with increasing spatial resolution. Based on the work of Bauer-
361 Marschallinger et al. (2018) and others, the radar signal has a large noise (speckle effect) at the
362 field scale due to the interference with heterogeneous vegetation, terrain surface, and soil
363 properties. Upscaling Sentinel-1 data to a larger spatial resolution (e.g. 500 m) is required to
364 reduce the sensor's noise. As such, the SSM established here may not be transformed to a finer
365 resolution without reducing the model performance. To delineate the SSM variations at such a
366 fine resolution (e.g. plot scale, Figure 8), soil core sampling (Li et al., 2019) or ground-based
367 proximal soil sensors (Robinson et al., 2008; Striegl and Loheide, 2012) should be used instead.

368 **Fig. 8 (near here)**

369

370 4.3. Irrigation Management at the Field Scale via Data Fusion of Remote Sensing and Land 371 Surface Parameters Data

372 Compared to traditional in situ soil moisture sensors that are installed on the farm to monitor
373 SSM at limited individual stations or SMAP_L3 SSM products (e.g. radiometer) that rely on
374 space-borne sensors to monitor SSM with a very coarse resolution (36 km), the retrieved SSM
375 maps can delineate field-scale variations in SSM (Figures 5 and 7), which can be potentially used
376 for monitoring SSM and irrigation scheduling at the field scale. The maps of SSM identify
377 regions with a high irrigation priority and the pixel resolution ($100\text{ m} \times 100\text{ m}$: 1 ha) is suitable
378 for irrigation management at the farm scale, whereby furrow irrigation is often used in this
379 region to supply water on a field by field basis.

380 In terms of the temporal resolution, the rate-limiting factor of the current SSM model is
381 the Sentinel-1 data, which are currently available 6–12 days globally (depending on the region of
382 interest). Future research is required to gap-fill the SSM maps within the 6–12 days to obtain
383 close to real-time SSM maps. This could be realized using space-time statistical method (Jost et
384 al., 2005) or mechanistic models (Or and Lehmann, 2019).

385 In addition, future research is required to map soil water content below the surface,
386 particularly within the root zone, as soil water content often varies greatly with depth within the
387 soil profile. This can be potentially achieved by data assimilation of the empirical machine
388 learning SSM model with a mechanistic water balance model (e.g. Das and Mohanty, 2006;
389 Huang et al., 2017). Alternatively, to calculate soil water stored within the root zone, empirical
390 and analytical models can be established based on the retrieved SSM maps over a long-term
391 period (Arya et al., 1983; Jackson et al., 1987; Wagner et al., 1999; Gouweleeuw, 2000; Jackson,
392 2002; Ceballos et al., 2005; Albergel et al. 2008; Sadeghi et al., 2019a,b).

393

394 4.4. Developing an Additive and Adaptable SSM Model via Machine Learning

395 Only small numbers of the validation stations were available for certain land cover types (e.g.
396 grassland in OZNET and REMEDHUS, and shrubland and forest in all networks). This could
397 contribute to the moderate performance of QRF model under these land cover types because
398 machine learning algorithms often require a large number of training dataset to capture the
399 variations in the model response (i.e. SSM) and the feature space (i.e. environmental covariates).
400 The accuracy of the SSM model also needs to be further improved in cropped areas where
401 accurate characterization of soil water conditions is crucial for sustaining crop yield and
402 maximizing water use efficiency.

403 Additional SSM measurements from vegetation-specific (e.g. cotton, olives, vegetables,
404 fruits) ground soil moisture networks should be collected to provide dataset covering these
405 feature spaces to improve the empirical QRF model. This is equivalent to the “spiking”
406 techniques used to calibrate the global soil visible near-infrared spectroscopy library using local
407 spectra data (Guerrero et al., 2010; Wetterlind and Stenberg, 2010; Viscarra Rossel et al., 2016).
408 In this regard, the empirical data fusion-based QRF model established here is an additive and
409 adaptable model and can be improved with addition of localized SSM measurements from in situ
410 soil moisture networks in the future.

411 **Fig. 9 (near here)**

412

413 **5. Conclusions**

414 An empirical surface soil moisture (SSM) model was established via data fusion of remote
415 sensing data (Sentinel-1 and SMAP) and land surface parameters (e.g. soil texture, terrain
416 parameters) using quantile random forest (QRF) algorithm. The model had a spatial resolution of
417 100 m and performed moderately well ($R^2 = 0.53$, $RMSE = 0.08 \text{ m}^3 \text{ m}^{-3}$) across the globe under
418 cropland, grassland, savanna, barren, and forest soils. Particularly, the empirical QRF model
419 performed better than the 36-km SMAP SSM model under cropland and savanna soils.

420 SSM was retrieved and mapped at 100 m every 6-12 days during the plant growing
421 seasons in 2018 in selected cropland and grassland fields in the OZNET network, Australia. It
422 was concluded that the high-resolution SSM maps can be used to monitor soil water content at
423 the field scale for irrigation management. The SSM model is an additive and adaptable model,
424 which can be further improved by including soil moisture measurements at the field scale for
425 specific vegetation/crop types. Further research is required to improve the temporal resolution of
426 the SSM model and map soil water content within the root zone.

427

428 **Acknowledgments**

429 We acknowledge the USDA Hatch project for providing support for the project. We
430 acknowledge HOBE, OZNET, REMEDHUS, SCAN, USCRN, National Soil Moisture Network,
431 and International Soil Moisture Network for providing the surface soil moisture measurements.
432 We acknowledge SoilGrids & Openlandmap, NASA, and US Geological Survey for providing
433 maps of land surface parameters. We also acknowledge ESA and NASA for providing land
434 surface and soil moisture products. The R codes for the quantile random forest model, training
435 datasets, and ancillary data for soil moisture mapping in Australia are available at the Zenodo
436 repository (DOI: 10.5281/zenodo.3659192).

437

438 **References**

439 Bauer-Marschallinger, B., Freeman, V., Cao, S., Paulik, C., Schaufler, S., Stachl, T., ... &
440 Wagner, W. (2018). Toward global soil moisture monitoring with Sentinel-1: Harnessing

441 assets and overcoming obstacles. *IEEE Transactions on Geoscience and Remote Sensing*,
442 57(1), 520-539. <https://doi.org/10.1109/TGRS.2018.2858004>

443 BBC, 2018. New South Wales drought now affects entire state. Accessed from
444 <https://www.bbc.com/news/world-australia-45107504>

445 Bigiarini, M. Z., & Bigiarini, M. M. Z. (2013). Package “hydroGOF”. R-package, available at:
446 [www. r-project.org/](http://www.r-project.org/)(last access: 7 Jan 2020).

447 Bureau of Meteorology, 2018. Map of root-zone soil moisture for the previous month. Accessed
448 from [http://www.bom.gov.au/climate/drought/archive/20181205.archive.shtml#tabs2=Soil-](http://www.bom.gov.au/climate/drought/archive/20181205.archive.shtml#tabs2=Soil-moisture)
449 [moisture](http://www.bom.gov.au/climate/drought/archive/20181205.archive.shtml#tabs2=Soil-moisture)

450 Das, N. N., Entekhabi, D., Dunbar, R. S., Chaubell, M. J., Colliander, A., Yueh, S., ... & Walker,
451 J. P. (2019). The SMAP and Copernicus Sentinel 1A/B microwave active-passive high
452 resolution surface soil moisture product. *Remote Sensing of Environment*, 233, 111380.
453 <https://doi.org/10.1016/j.rse.2019.111380>

454 Dorigo, W. A., Wagner, W., Hohensinn, R., Hahn, S., Paulik, C., Xaver, A., ... & Robock, A.
455 (2011). The International Soil Moisture Network: a data hosting facility for global in situ
456 soil moisture measurements. *Hydrology and Earth System Sciences*, 15(5), 1675-1698.
457 <https://doi.org/10.5194/hess-15-1675-2011>

458 Dubois, P. C., Van Zyl, J., & Engman, T. (1995). Measuring soil moisture with imaging radars.
459 *IEEE Transactions on Geoscience and Remote Sensing*, 33(4), 915-926.

460 Entekhabi, D., Njoku, E. G., O'Neill, P. E., Kellogg, K. H., Crow, W. T., Edelstein, W. N., ... &
461 Kimball, J. (2010). The soil moisture active passive (SMAP) mission. *Proceedings of the*
462 *IEEE*, 98(5), 704-716.

463 Fisher, J. B., Melton, F., Middleton, E., Hain, C., Anderson, M., Allen, R., ... & Kilic, A. (2017).
464 The future of evapotranspiration: Global requirements for ecosystem functioning, carbon
465 and climate feedbacks, agricultural management, and water resources. *Water Resources*
466 *Research*, 53(4), 2618-2626. <https://doi.org/10.1002/2016WR020175>

467 Fung, A. (1994), *Microwave Scattering and Emission Models and Their Applications*, Artech
468 House, Boston, Mass.

469 Friedl, M. A., Sulla-Menashe, D., Tan, B., Schneider, A., Ramankutty, N., Sibley, A., & Huang,
470 X. (2010). MODIS Collection 5 global land cover: Algorithm refinements and
471 characterization of new datasets. *Remote sensing of Environment*, 114(1), 168-182.

472 <https://doi.org/10.1016/j.rse.2009.08.016>

473 Gao, Q., Zribi, M., Escorihuela, M., & Baghdadi, N. (2017). Synergetic use of Sentinel-1 and
474 Sentinel-2 data for soil moisture mapping at 100 m resolution. *Sensors*, 17(9), 1966.
475 <https://doi.org/10.3390/s17091966>

476 Grundy, M. J., Rossel, R. V., Searle, R. D., Wilson, P. L., Chen, C., & Gregory, L. J. (2015). Soil
477 and landscape grid of Australia. *Soil Research*, 53(8), 835-844.
478 <https://doi.org/10.1071/SR15191>

479 Guerrero, C., Zornoza, R., Gómez, I., & Mataix-Beneyto, J. (2010). Spiking of NIR regional
480 models using samples from target sites: Effect of model size on prediction accuracy.
481 *Geoderma*, 158(1-2), 66-77. <https://doi.org/10.1016/j.geoderma.2009.12.021>

482 Guevara, M., & Vargas, R. (2019). Downscaling satellite soil moisture using geomorphometry
483 and machine learning. *PLoS one*, 14(9), e0219639.
484 <https://doi.org/10.1371/journal.pone.0219639>

485 Hengl, T., de Jesus, J. M., Heuvelink, G. B., Gonzalez, M. R., Kilibarda, M., Blagotić, A., ... &
486 Guevara, M. A. (2017). SoilGrids250m: Global gridded soil information based on machine
487 learning. *PLoS one*, 12(2). <https://doi.org/10.1371/journal.pone.0169748>

488 Hengl, T., & Gupta, S. (2019). Soil water content (volumetric %) for 33kPa and 1500kPa
489 suctions predicted at 6 standard depths (0, 10, 30, 60, 100 and 200 cm) at 250 m resolution
490 (Version v01) [Data set]. Zenodo. 10.5281/zenodo.2629589

491 Janis, M. J., & Center, S. R. C. (2002). US Climate Reference Network (USCRN) Site
492 Identification, Survey, and Selection FY 02 Research Project for The NOAA Regional
493 Climate Centers (RCC).

494 Jensen, K. H., & Illangasekare, T. H. (2011). HOBE: A hydrological observatory. *Vadose Zone*
495 *Journal*, 10(1), 1-7. <https://doi.org/10.2136/vzj2011.0006>

496 Jost, G., Heuvelink, G. B. M., & Papritz, A. (2005). Analysing the space–time distribution of soil
497 water storage of a forest ecosystem using spatio-temporal kriging. *Geoderma*, 128(3-4),
498 258-273. <https://doi.org/10.1016/j.geoderma.2005.04.008>

499 Li, X., Shao, M., Zhao, C., Liu, T., Jia, X., & Ma, C. (2019). Regional spatial variability of root-
500 zone soil moisture in arid regions and the driving factors - A case study of Xinjiang, China.
501 *Canadian Journal of Soil Science*, 99(3), 277-291. <https://doi.org/10.1139/cjss-2019-0006>

502 Lievens, H., Reichle, R. H., Liu, Q., De Lannoy, G. J. M., Dunbar, R. S., Kim, S. B., ... &

503 Wagner, W. (2017). Joint Sentinel-1 and SMAP data assimilation to improve soil moisture
504 estimates. *Geophysical Research Letters*, 44(12), 6145-6153.
505 <https://doi.org/10.1002/2017GL073904>

506 Martínez-Fernández, J., & Ceballos, A. (2005). Mean soil moisture estimation using temporal
507 stability analysis. *Journal of Hydrology*, 312(1-4), 28-38.
508 <https://doi.org/10.1016/j.jhydrol.2005.02.007>

509 Meinshausen, N. (2006). Quantile regression forests. *Journal of Machine Learning Research*,
510 7(Jun), 983-999. Available on
511 <http://www.jmlr.org/papers/volume7/meinshausen06a/meinshausen06a.pdf>

512 Meinshausen, N., & Meinshausen, M. N. (2017). Package ‘quantregForest’, version 1.3-7.

513 Merzouki, A., McNairn, H., & Pacheco, A. (2011). Mapping soil moisture using RADARSAT-2
514 data and local autocorrelation statistics. *IEEE Journal of Selected Topics in Applied Earth
515 Observations and Remote Sensing*, 4(1), 128-137.
516 <https://doi.org/10.1109/JSTARS.2011.2116769>

517 Oh, Y., Sarabandi, K., & Ulaby, F. T. (1992). An empirical model and an inversion technique for
518 radar scattering from bare soil surfaces. *IEEE transactions on Geoscience and Remote
519 Sensing*, 30(2), 370-381. <https://doi.org/10.1109/36.134086>

520 Olaya, V. (2009). Basic land-surface parameters. *Developments in Soil Science*, 33, 141-169.
521 [https://doi.org/10.1016/S0166-2481\(08\)00006-8](https://doi.org/10.1016/S0166-2481(08)00006-8)

522 O’Neill, P. E., Njoku, E. G., Jackson, T. J., Chan, S., & Bindlish, R. (2015). SMAP algorithm
523 theoretical basis document: Level 2 & 3 soil moisture (passive) data products. Jet Propulsion
524 Lab., California Inst. Technol., Pasadena, CA, USA, JPL D-66480.

525 Or, D., & Lehmann, P. (2019). Surface evaporative capacitance: How soil type and rainfall
526 characteristics affect global-scale surface evaporation. *Water Resources Research*, 55(1),
527 519-539. <https://doi.org/10.1029/2018WR024050>

528 Porporato, A., Daly, E., & Rodriguez-Iturbe, I. (2004). Soil water balance and ecosystem
529 response to climate change. *The American Naturalist*, 164(5), 625-632.
530 <https://doi.org/10.1086/424970>

531 Ochsner, T. E., Cosh, M. H., Cuenca, R. H., Dorigo, W. A., Draper, C. S., Hagimoto, Y., ... &
532 Larson, K. M. (2013). State of the art in large-scale soil moisture monitoring. *Soil Science
533 Society of America Journal*, 77(6), 1888-1919. <https://doi.org/10.2136/sssaj2013.03.0093>

534 Quiring, S. M., Ford, T. W., Wang, J. K., Khong, A., Harris, E., Lindgren, T., ... & Li, Z. (2016).
535 The North American soil moisture database: Development and applications. *Bulletin of the*
536 *American Meteorological Society*, 97(8), 1441-1459. [https://doi.org/10.1175/BAMS-D-13-](https://doi.org/10.1175/BAMS-D-13-00263.1)
537 00263.1

538 Ramcharan, A., Hengl, T., Nauman, T., Brungard, C., Waltman, S., Wills, S., & Thompson, J.
539 (2018). Soil property and class maps of the conterminous United States at 100-meter spatial
540 resolution. *Soil Science Society of America Journal*, 82(1), 186-201.
541 <https://doi.org/10.2136/sssaj2017.04.0122>

542 Reuter, H. I., Nelson, A., & Jarvis, A. (2007). An evaluation of void-filling interpolation
543 methods for SRTM data. *International Journal of Geographical Information Science*, 21(9),
544 983-1008. <https://doi.org/10.1080/13658810601169899>

545 Robinson, D. A., Campbell, C. S., Hopmans, J. W., Hornbuckle, B. K., Jones, S. B., Knight, R.,
546 ... & Wendroth, O. (2008). Soil moisture measurement for ecological and hydrological
547 watershed-scale observatories: A review. *Vadose Zone Journal*, 7(1), 358-389.
548 <https://doi.org/10.2136/vzj2007.0143>

549 Sadeghi, M., Tuller, M., Warrick, A. W., Babaeian, E., Parajuli, K., Gohardoust, M. R., & Jones,
550 S. B. (2019). An analytical model for estimation of land surface net water flux from near-
551 surface soil moisture observations. *Journal of Hydrology*, 570, 26-37.
552 <https://doi.org/10.1016/j.jhydrol.2018.12.038>

553 Sadeghi, M., Ebtehaj, A., Crow, W. T., Gao, L., Purdy, A. J., Fisher, J. B., ... & Tuller, M.
554 (2019). Global Estimates of Land Surface Water Fluxes from SMOS and SMAP Satellite
555 Soil Moisture Data. *Journal of Hydrometeorology*, (2019). [https://doi.org/10.1175/JHM-D-](https://doi.org/10.1175/JHM-D-19-0150.1)
556 19-0150.1

557 Schaefer, G. L., Cosh, M. H., & Jackson, T. J. (2007). The USDA natural resources conservation
558 service soil climate analysis network (SCAN). *Journal of Atmospheric and Oceanic*
559 *Technology*, 24(12), 2073-2077. <https://doi.org/10.1175/2007JTECHA930.1>

560 Smith, A. B., Walker, J. P., Western, A. W., Young, R. I., Ellett, K. M., Pipunic, R. C., ... &
561 Richter, H. (2012). The Murrumbidgee soil moisture monitoring network data set. *Water*
562 *Resources Research*, 48(7).
563 <https://agupubs.onlinelibrary.wiley.com/doi/full/10.1029/2012WR011976>

564 Stoy, P. C., El-Madany, T., Fisher, J. B., Gentine, P., Gerken, T., Good, S. P., ... & Wohlfahrt12,

565 G. (2019). Reviews and syntheses: Turning the challenges of partitioning ecosystem
566 evaporation and transpiration into opportunities. *Biogeosciences Discussions*, 10.
567 <https://doi.org/10.5194/bg-16-3747-2019>

568 Striegl, A. M., & Loheide II, S. P. (2012). Heated distributed temperature sensing for field scale
569 soil moisture monitoring. *Groundwater*, 50(3), 340-347. [https://doi.org/10.1111/j.1745-
570 6584.2012.00928.x](https://doi.org/10.1111/j.1745-6584.2012.00928.x)

571 Trugman, A. T., Medvigy, D., Mankin, J. S., & Anderegg, W. R. L. (2018). Soil moisture stress
572 as a major driver of carbon cycle uncertainty. *Geophysical Research Letters*, 45(13), 6495-
573 6503. <https://doi.org/10.1029/2018GL078131>

574 Vereecken, H., Huisman, J. A., Pachepsky, Y., Montzka, C., Van Der Kruk, J., Bogaen, H., ... &
575 Vanderborght, J. (2014). On the spatio-temporal dynamics of soil moisture at the field scale.
576 *Journal of Hydrology*, 516, 76-96. <https://doi.org/10.1016/j.jhydrol.2013.11.061>

577 Viscarra Rossel, R., Behrens, T., Ben-Dor, E., Brown, D. J., Demattê, J. A. M., Shepherd, K. D.,
578 ... & Aichi, H. (2016). A global spectral library to characterize the world's soil. *Earth-
579 Science Reviews*, 155, 198-230. <https://doi.org/10.1016/j.earscirev.2016.01.012>

580 Wang, L., & Qu, J. J. (2009). Satellite remote sensing applications for surface soil moisture
581 monitoring: A review. *Frontiers of Earth Science in China*, 3(2), 237-247.
582 <https://doi.org/10.1007/s11707-009-0023-7>

583 Wei, J., & Dirmeyer, P. A. (2012). Dissecting soil moisture-precipitation coupling. *Geophysical
584 Research Letters*, 39(19). <https://doi.org/10.1029/2012GL053038>

585 Wetterlind, J., & Stenberg, B. (2010). Near-infrared spectroscopy for within-field soil
586 characterization: small local calibrations compared with national libraries spiked with local
587 samples. *European Journal of Soil Science*, 61(6), 823-843. [https://doi.org/10.1111/j.1365-
588 2389.2010.01283.x](https://doi.org/10.1111/j.1365-2389.2010.01283.x)

1 **Figure Captions**

2 **Figure 1.** Locations of regional-scale soil moisture monitoring networks HOBE (Denmark),
3 OZNET (Australia), REMEDHUS (Spain), and continental-scale soil moisture networks SCAN
4 and USCRN (USA). Note: Training and validation stations were highlighted in different colors.

5 **Figure 2.** Flowchart of the global surface soil water model established using data fusion and
6 machine learning.

7 **Figure 3.** Variable importance of the quantile random forest (QRF) model and a comparison of
8 model performance on training and validation datasets generated based on data fusion based
9 QRF model and SMAP-L3 surface soil moisture (SSM) product.

10 **Figure 4.** Plots of measured surface soil moisture (SSM) (black lines) under various land cover
11 types at several soil moisture stations and estimated SSM from SMAP (blue lines) and the data
12 fusion based quantile random forest (QRF) model (red lines, with 5 and 95 percentiles marked in
13 dashed lines). Note: no SSM estimates were made during October to February.

14 **Figure 5.** Predicted surface soil moisture (SSM, $m^3 m^{-3}$) from the quantile random forest (QRF)
15 model during the 2018 cropping season across selected fields within OZNET network in New
16 South Wales, Australia.

17 **Figure 6.** Maps of MODIS estimated cumulative gross primary productivity (GPP, $g C m^{-2}$ per
18 8-day), evapotranspiration (ET, $mm H_2O$ per 8-day), and water use efficiency (WUE, $g C$ per
19 $mm H_2O$) during the 2018 growing season across selected fields within OZNET network in New
20 South Wales, Australia.

21 **Figure 7.** Plots of measured and predicted surface soil moisture (SSM, $m^3 m^{-3}$) from the quantile
22 random forest (QRF) model and NASA-SMAP, MODIS cumulative gross primary productivity
23 (GPP, $g C m^{-2}$ per 8-day), evapotranspiration (ET, $mm H_2O$ per 8-day), and water use efficiency
24 (WUE, $g C$ per $mm H_2O$) at three selected sites (irrigated cropland 1 and 2, rainfed grassland)
25 during the 2018 growing season within OZNET network in New South Wales, Australia.

26 **Figure 8.** Spatial and temporal resolutions of current remote sensing soil moisture monitoring
27 satellites. Note: satellites used in this study are highlighted in black and other satellites designed
28 to monitor soil moisture are marked in grey.

29

Figure1.

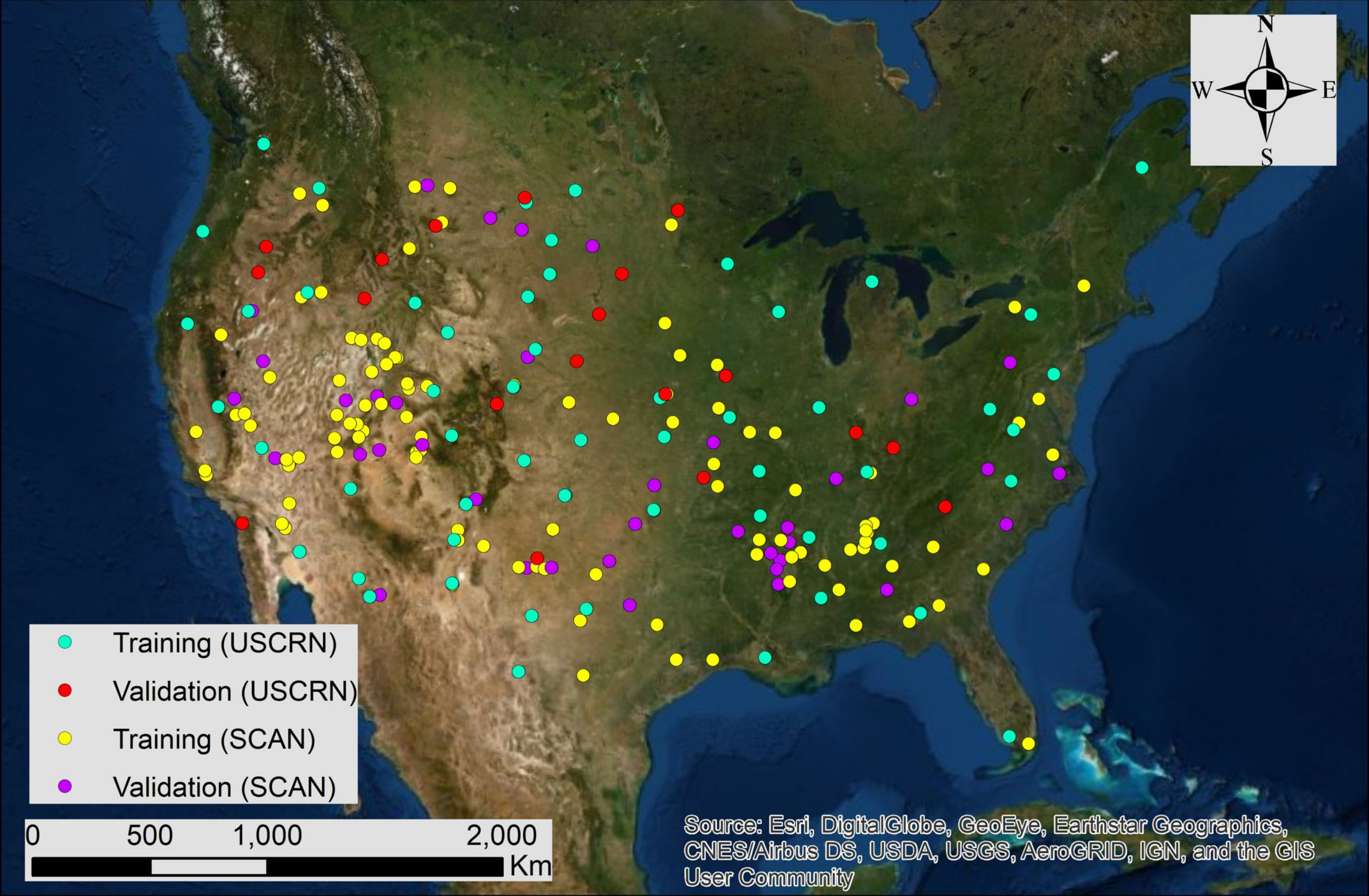
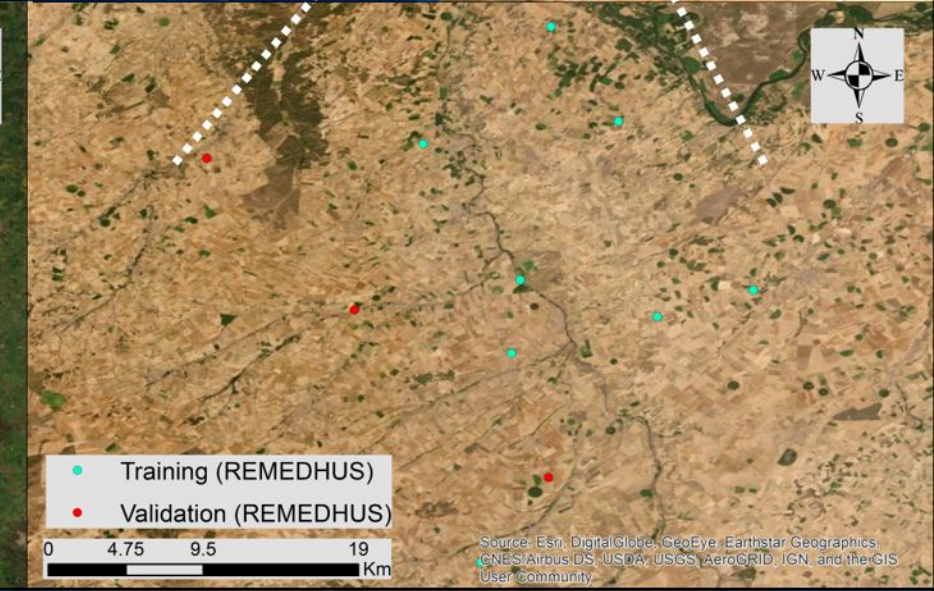
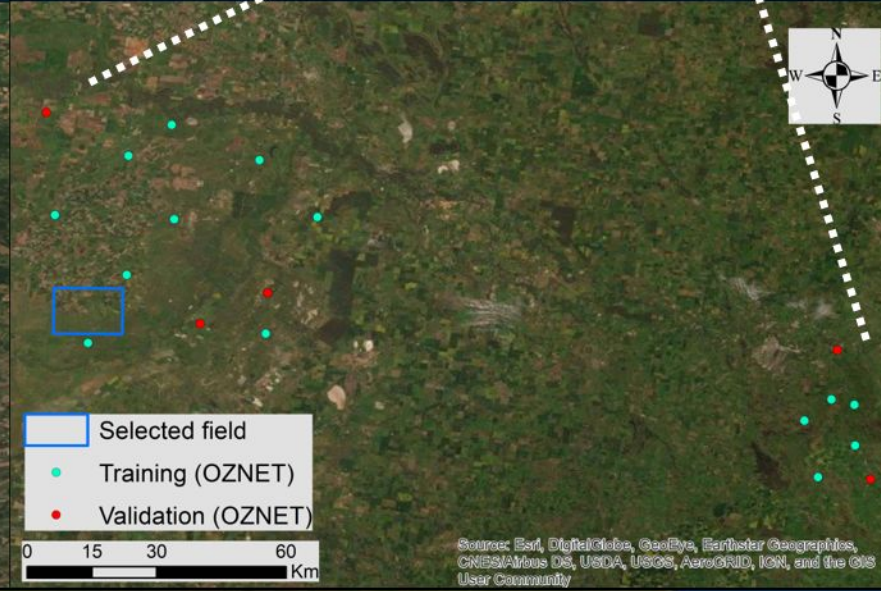
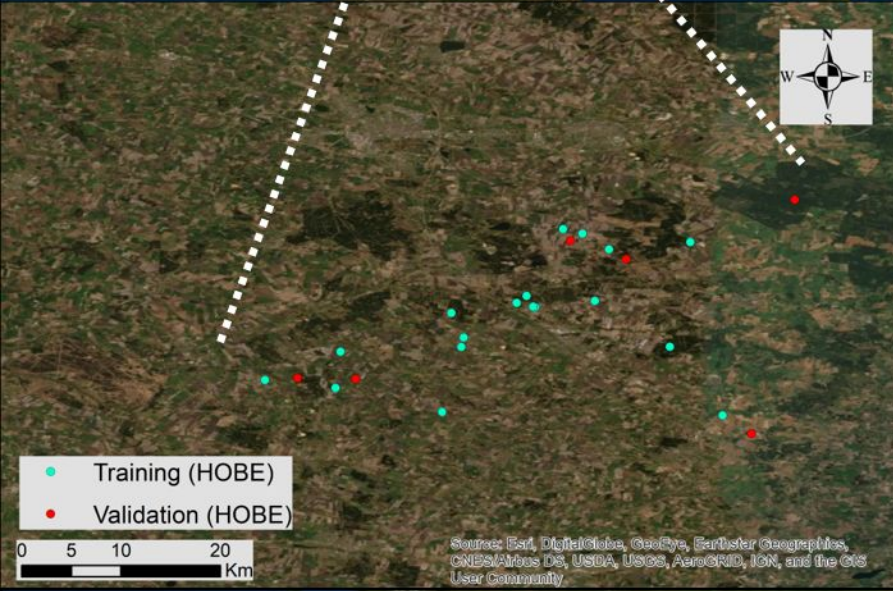
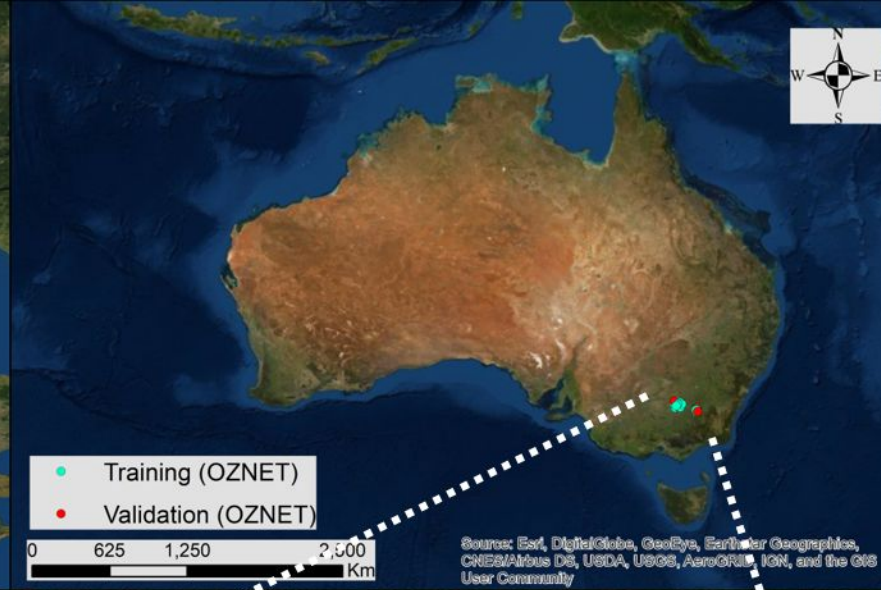


Figure2.

Ground SSM measurements

Regional-scale SSM networks: HOBE, OZNET, REMEDHUS

Continental-scale SSM networks: SCAN, USCRN

Time-varying covariates

NASA SMAP (L3_SM_P):
SSM (36 km, 2-3 days)

ESA Sentinel-1 (VV & VH):
backscatter & incident angle (100 m, 6-12 days)

Time-constant covariates

ESA Sentinel-1 (VV & VH): temporal statistics (100 m)

GMTED2010 DEM: terrain parameters (250 m)

SoilGrids: clay, sand, BD, SOC, FC, PWP (250 m)

Training (75%):

Cropland, Grassland, Savanna,
Shrubland, Forest, Barren

Validation (25%):

Cropland, Grassland, Savanna,
Shrubland, Forest, Barren

Data fusion & machine learning: quantile random forest

Predicted mean and SD of SSM (100 m, 6-12 days)

Figure3.

SMAP
 sand
 VV
 VH
 Angle
 VH (Mean)
 TRI
 TPI
 Aspect
 Clay
 VV (Mean)
 VV (Min)
 Slope
 BD
 SOC
 FC
 PWP
 VV (SD)
 VH (Min)
 VH (Max)
 VH (SD)
 Flow direction

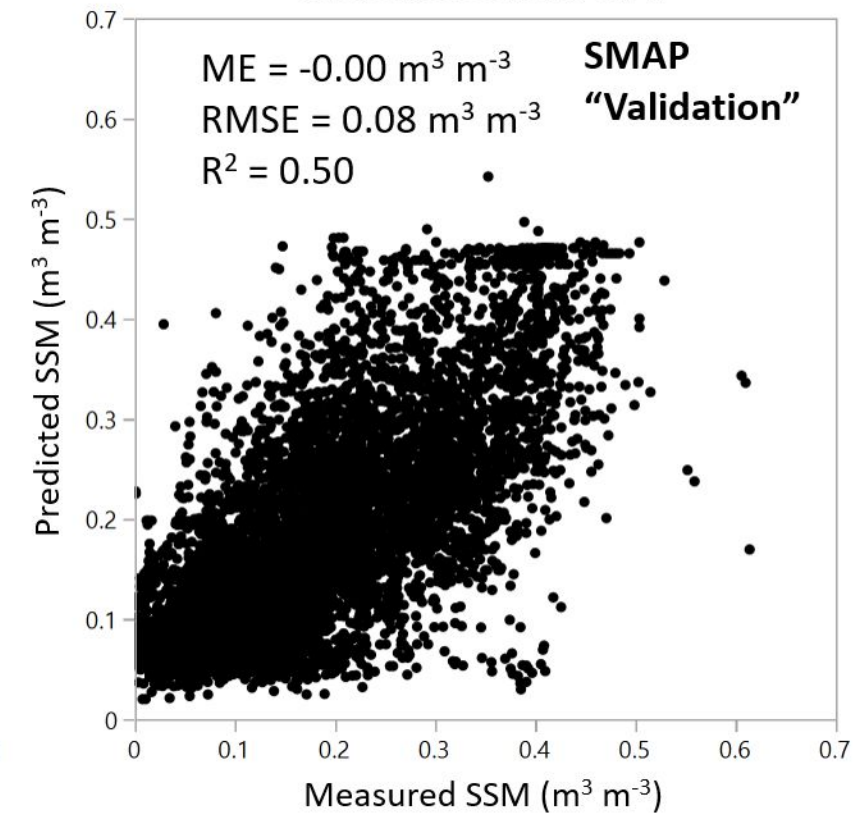
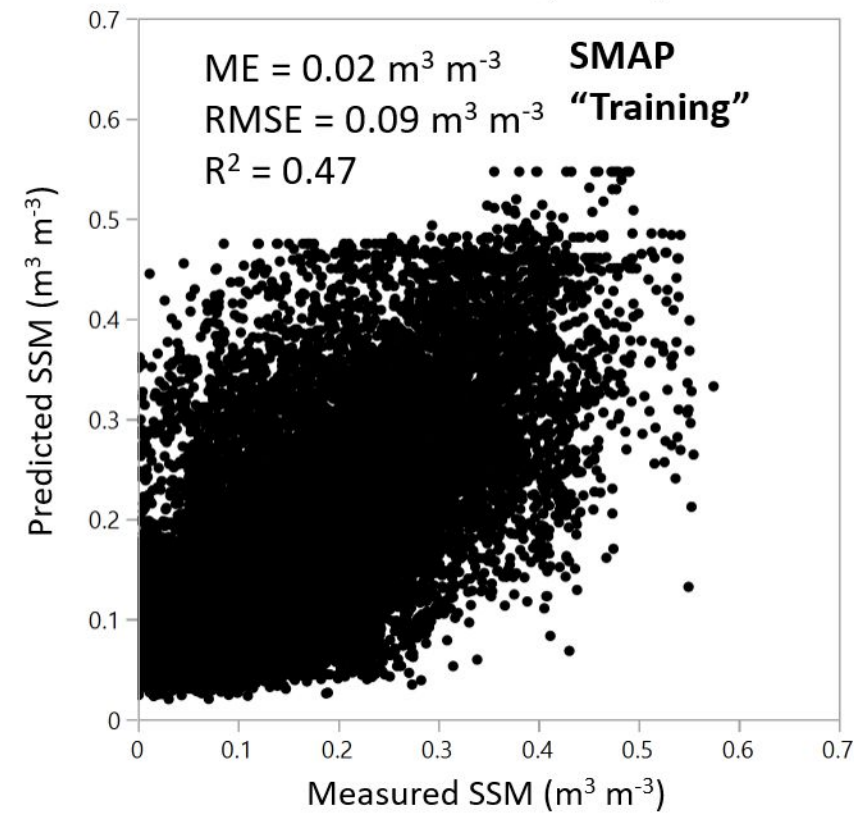
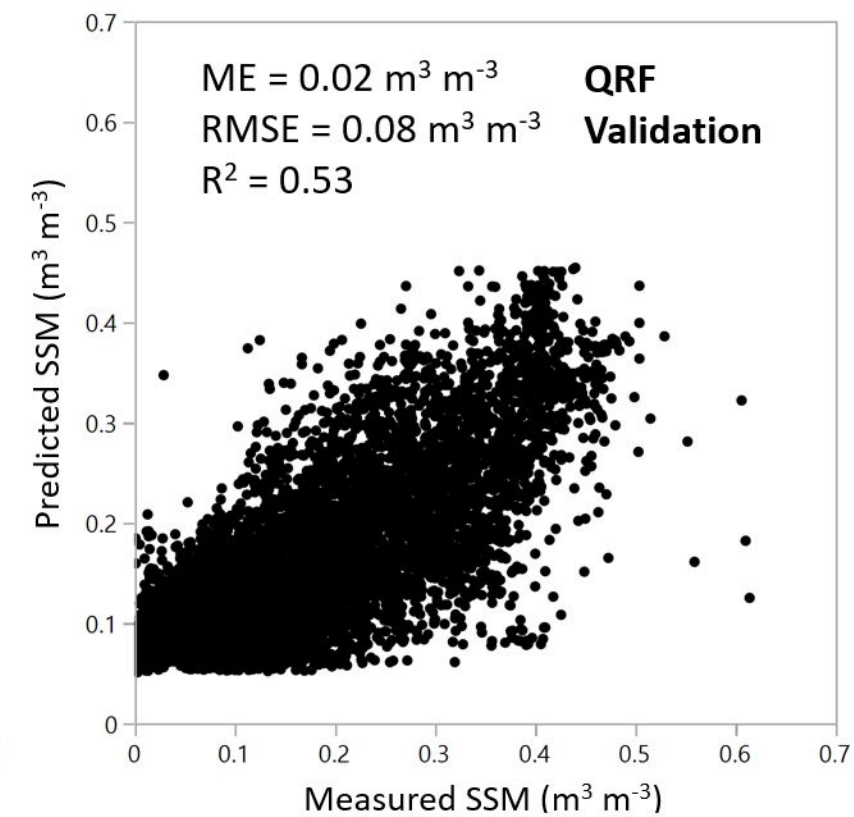
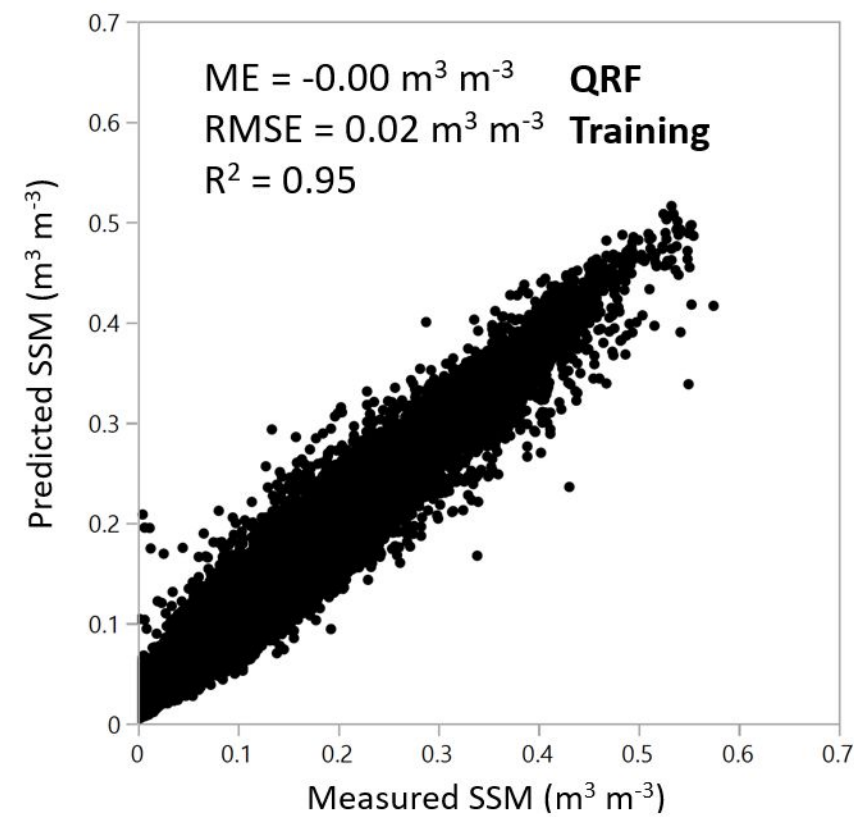
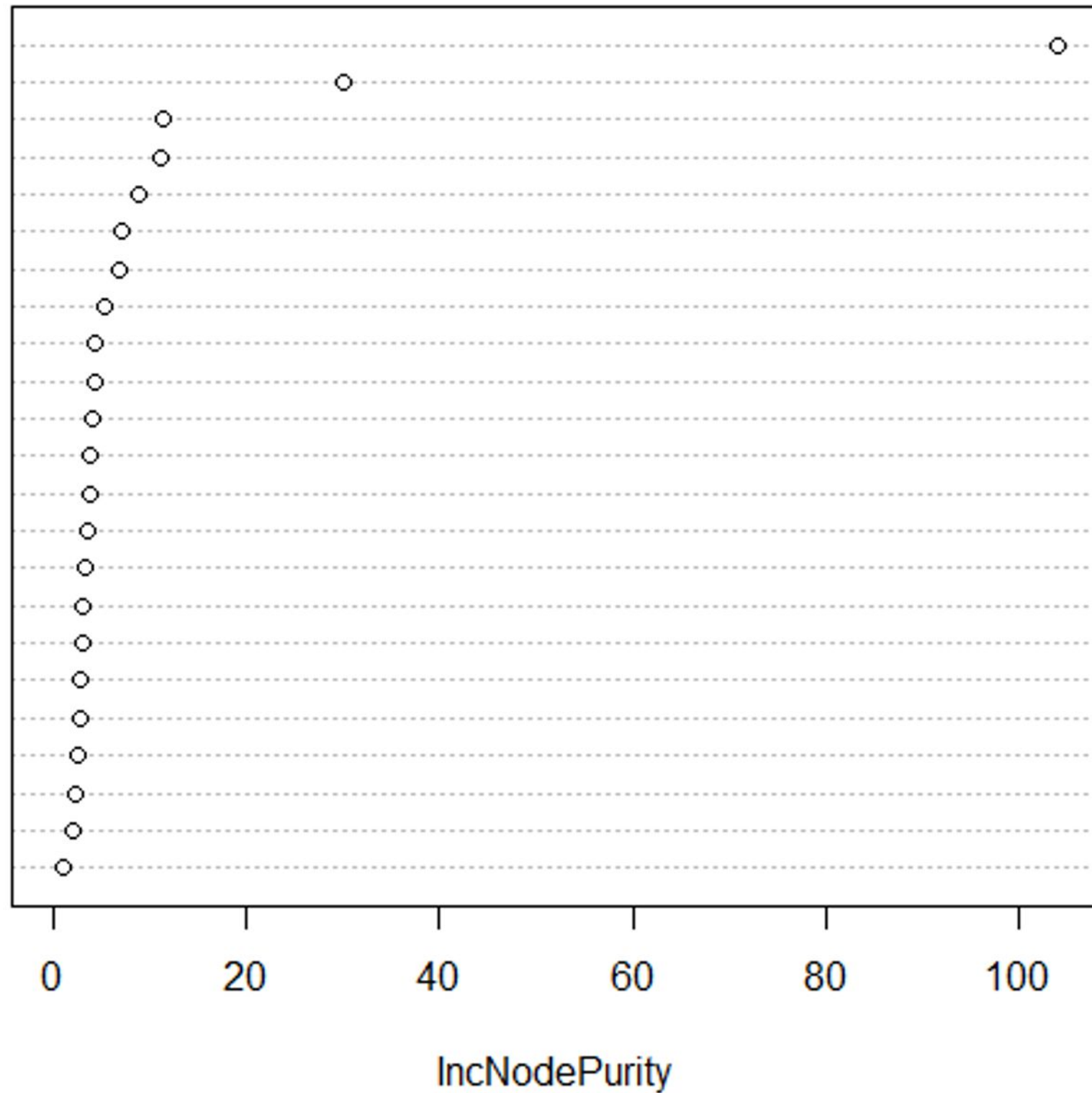


Figure4.

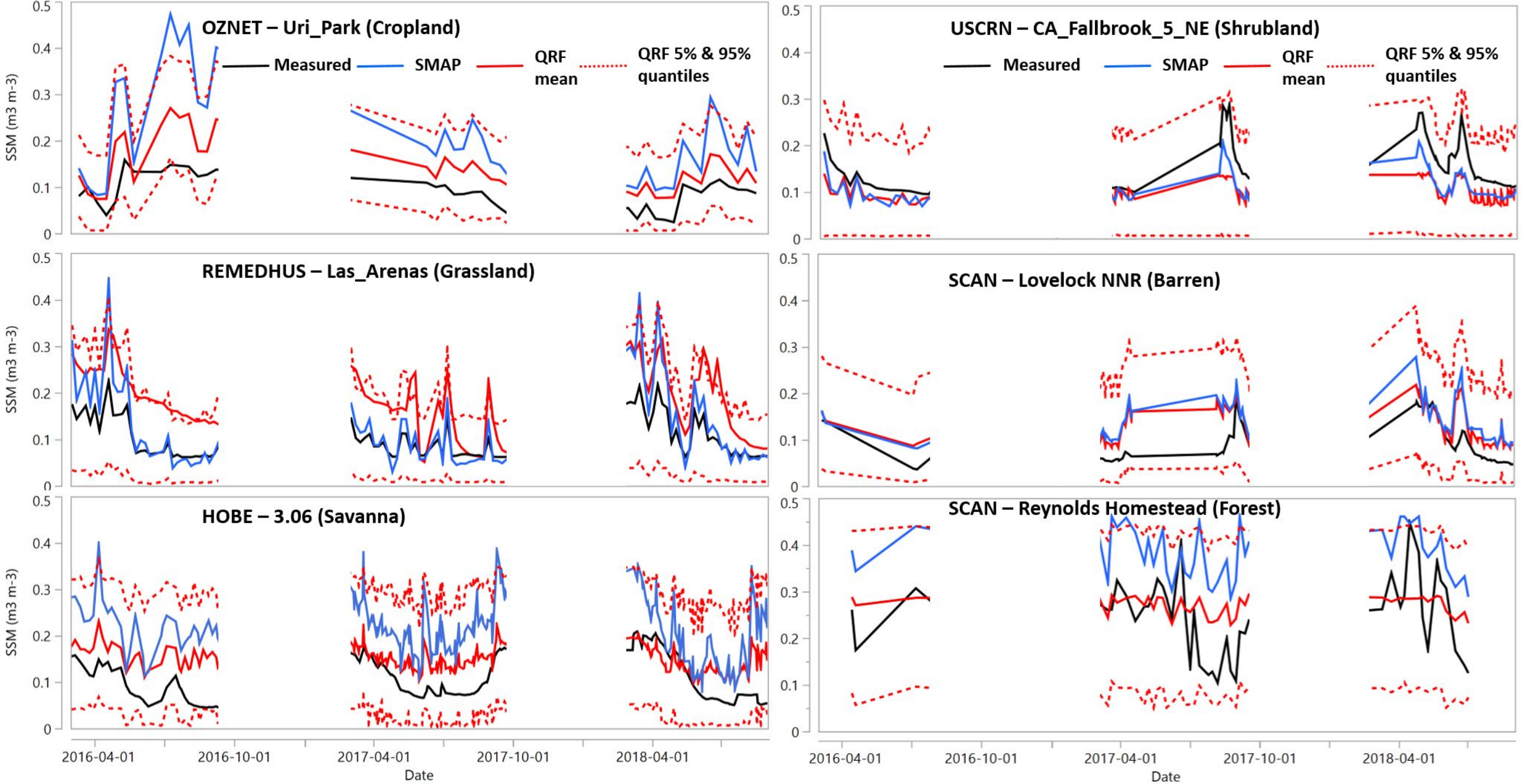


Figure 5.

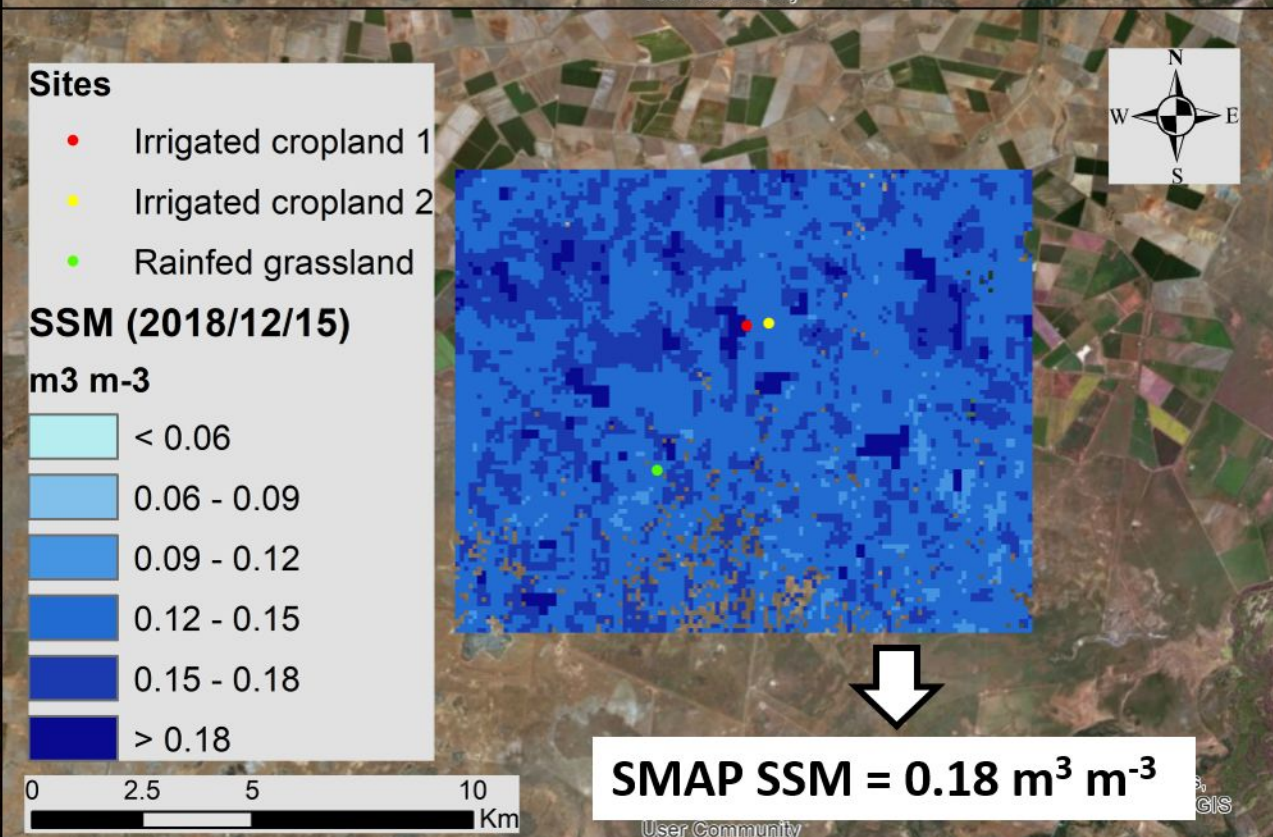
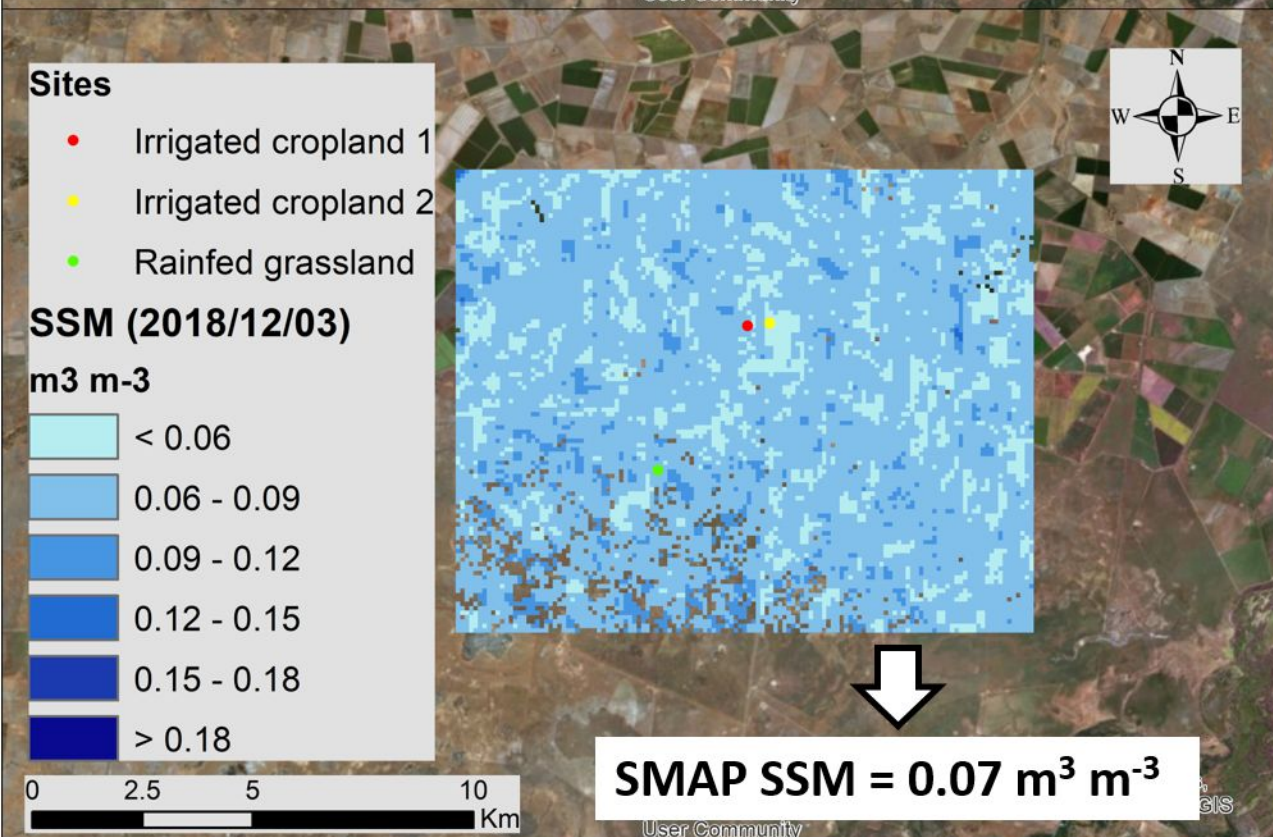
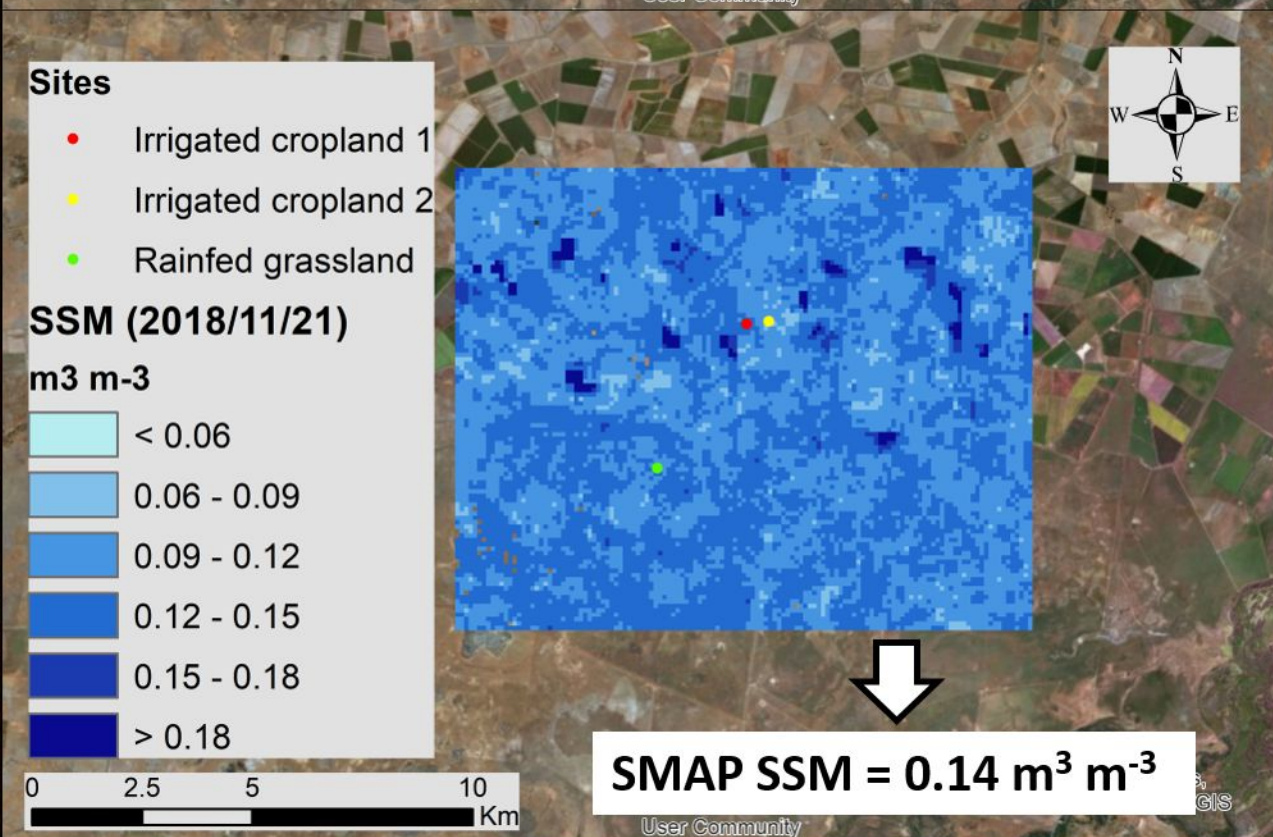
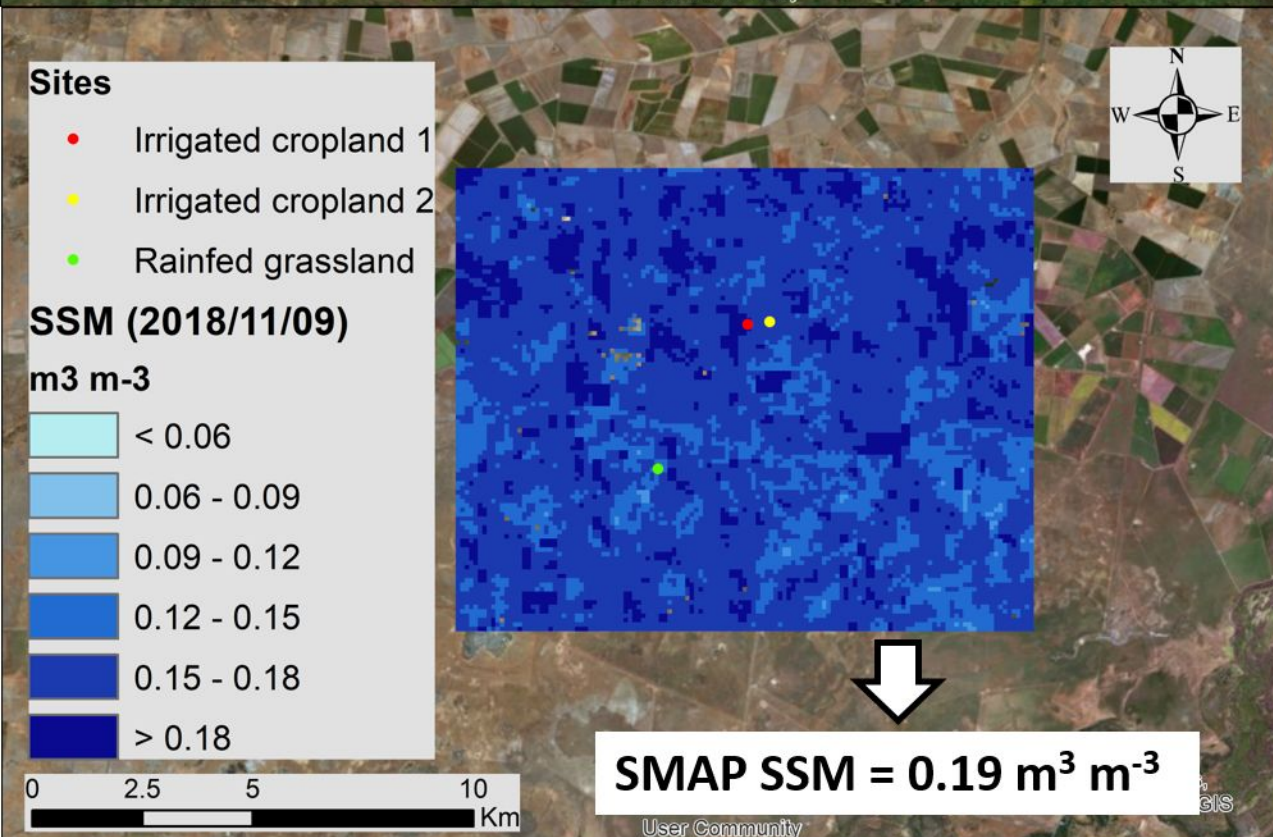
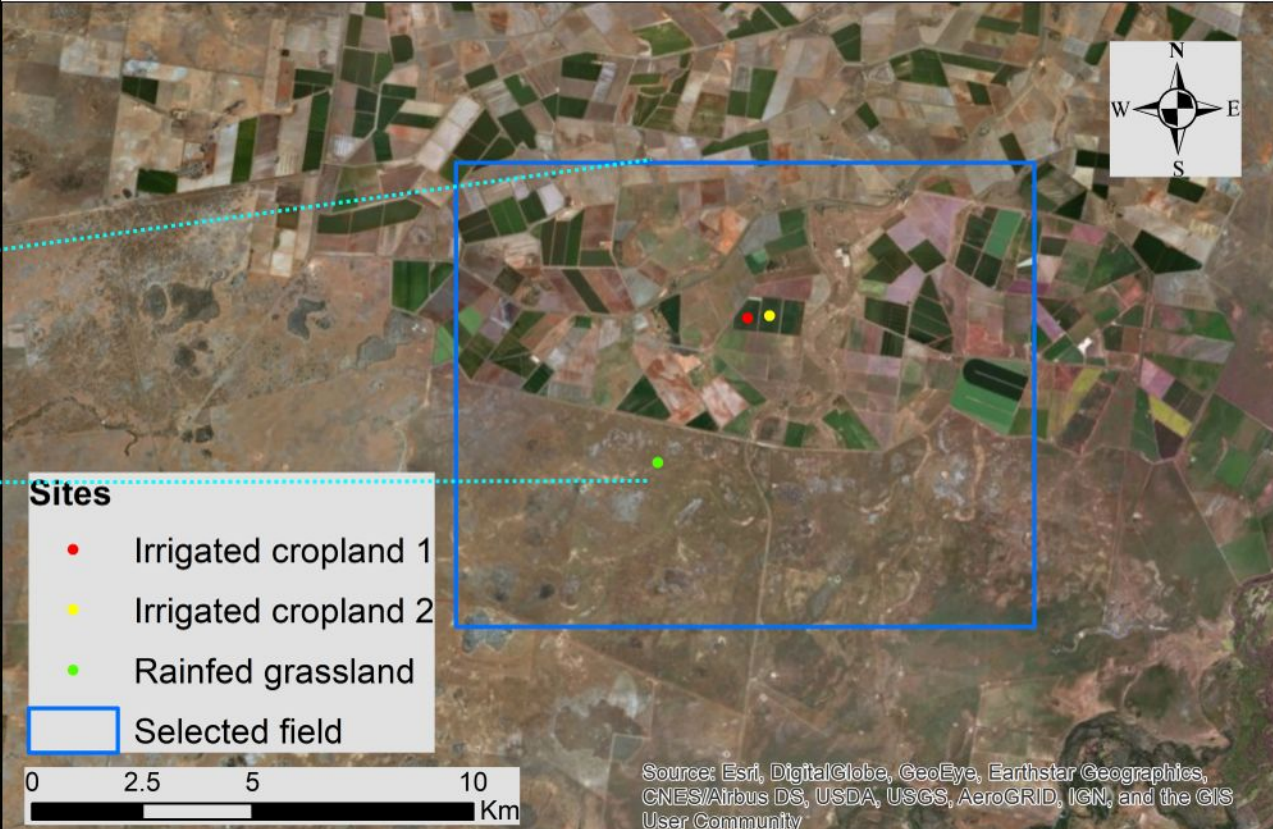
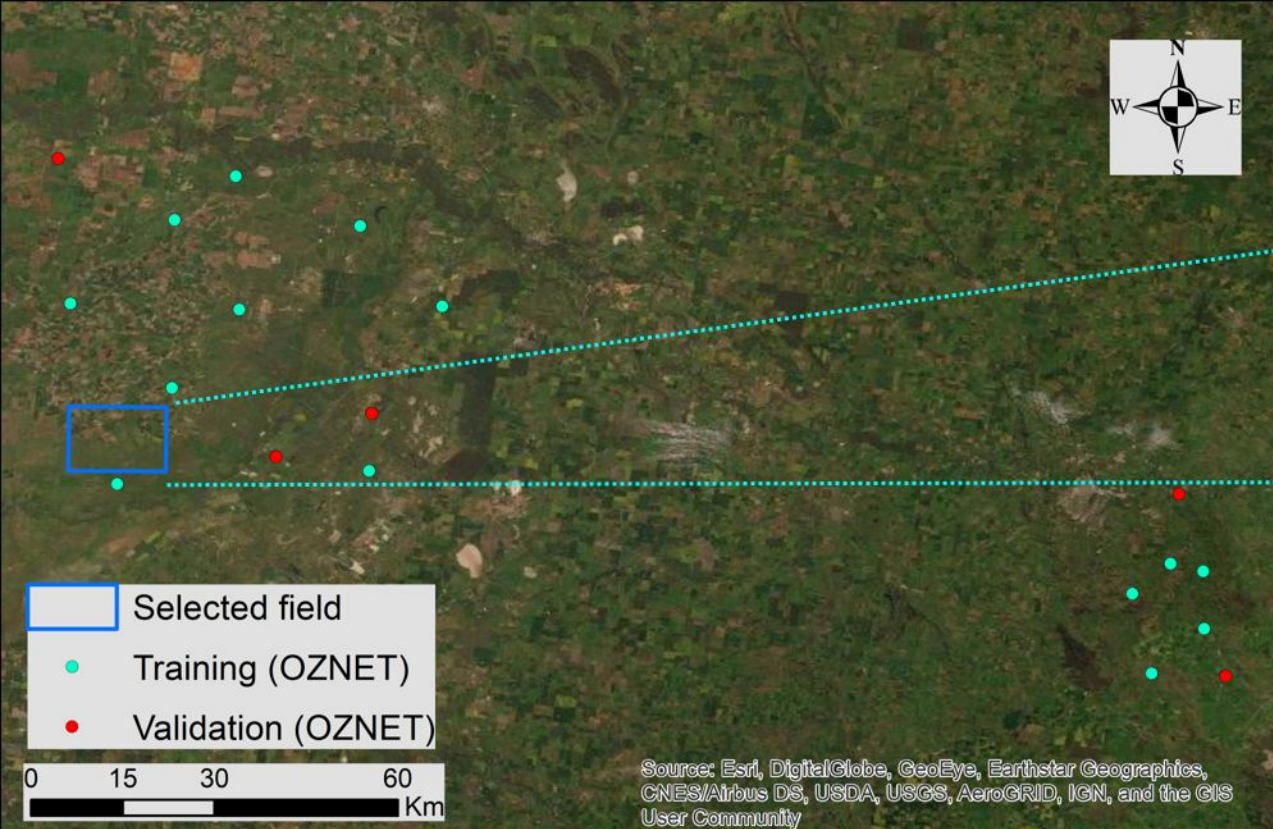


Figure6.

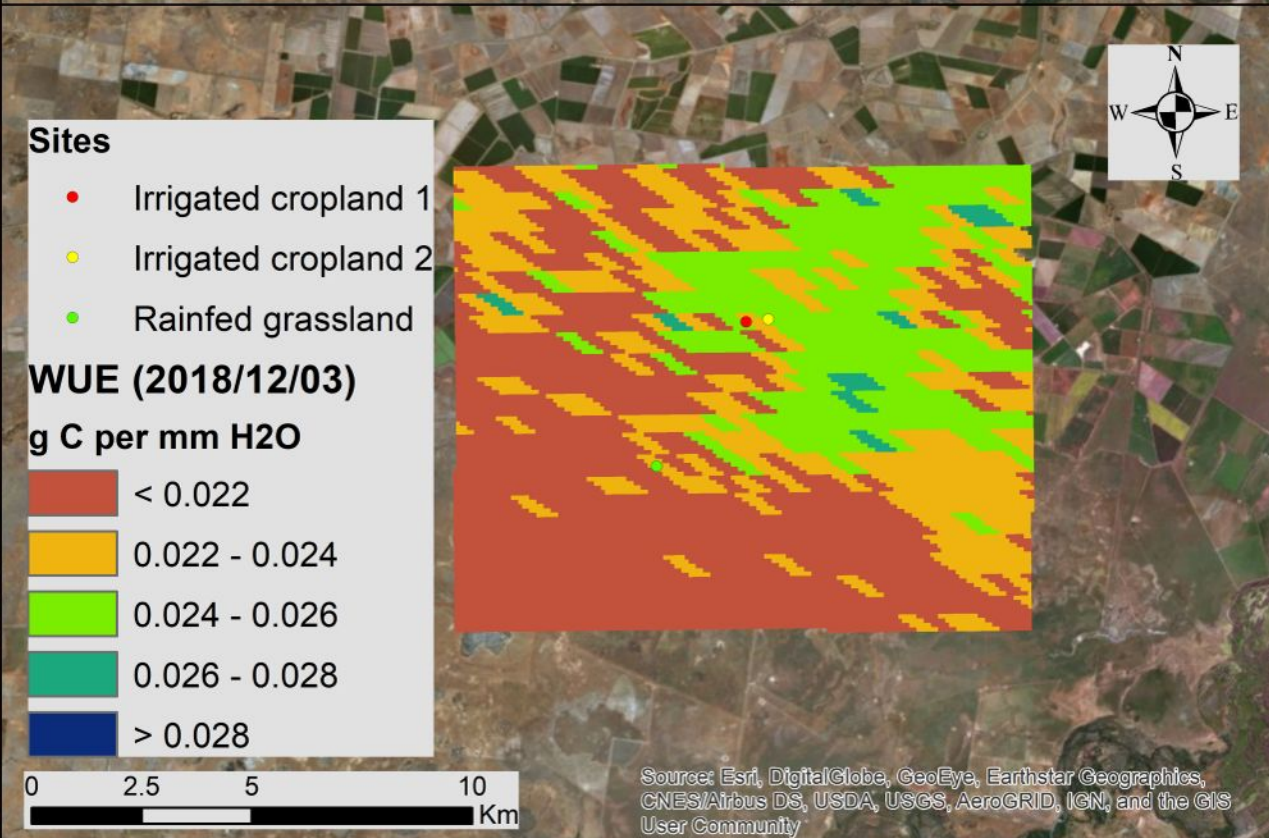
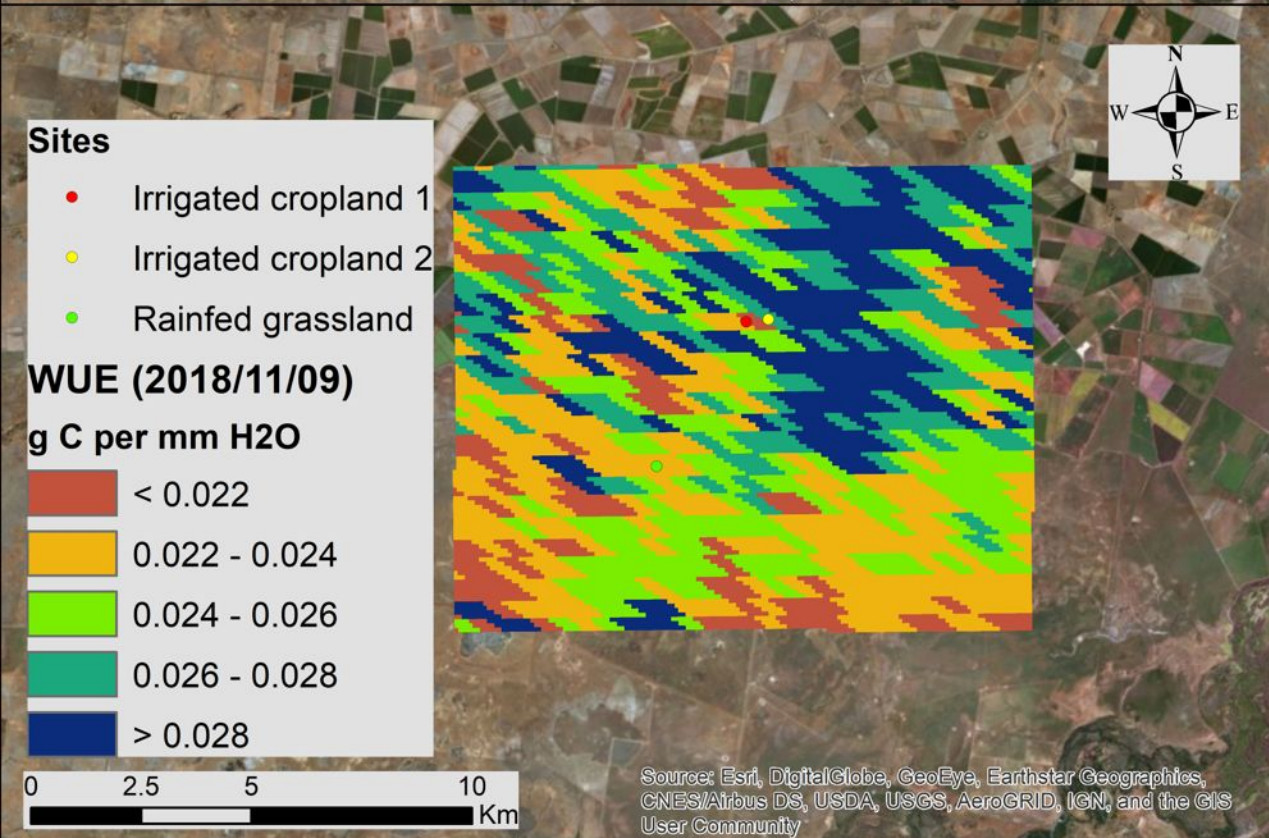
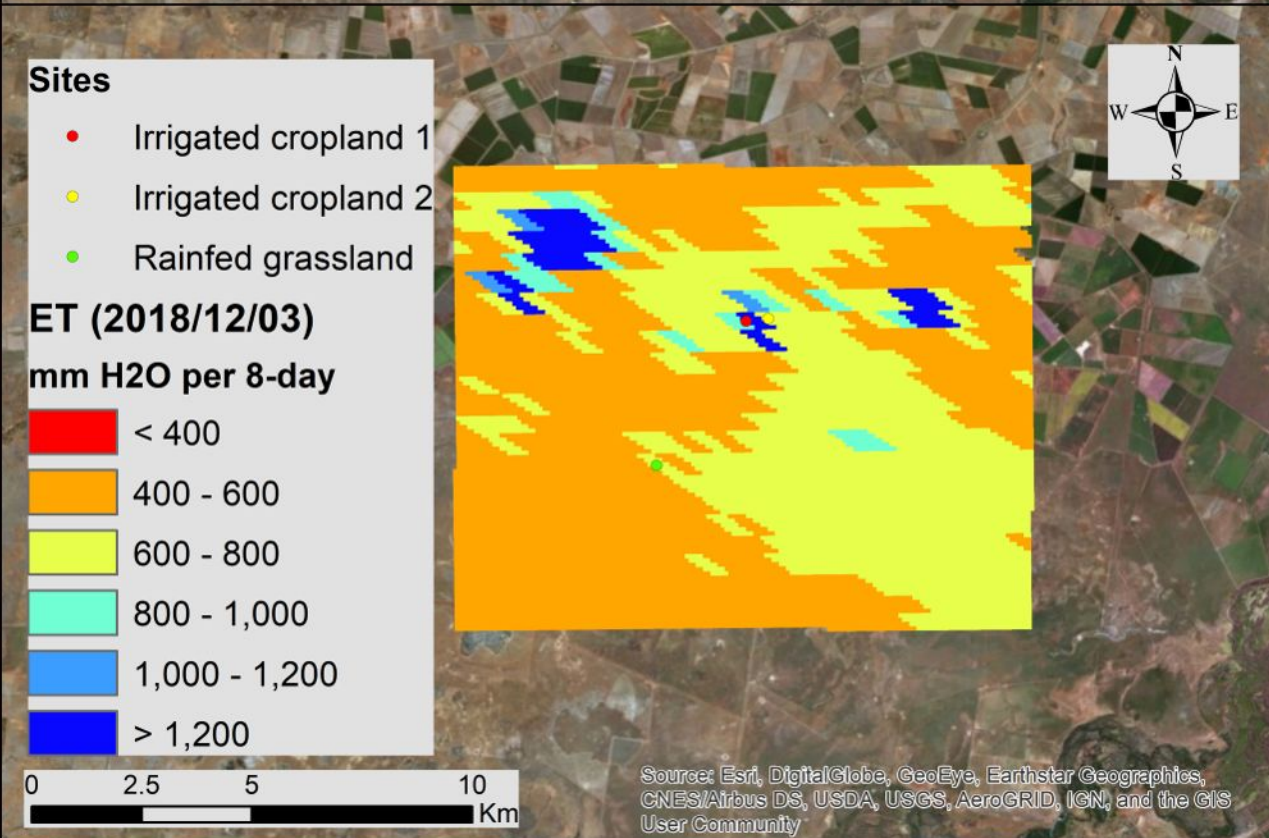
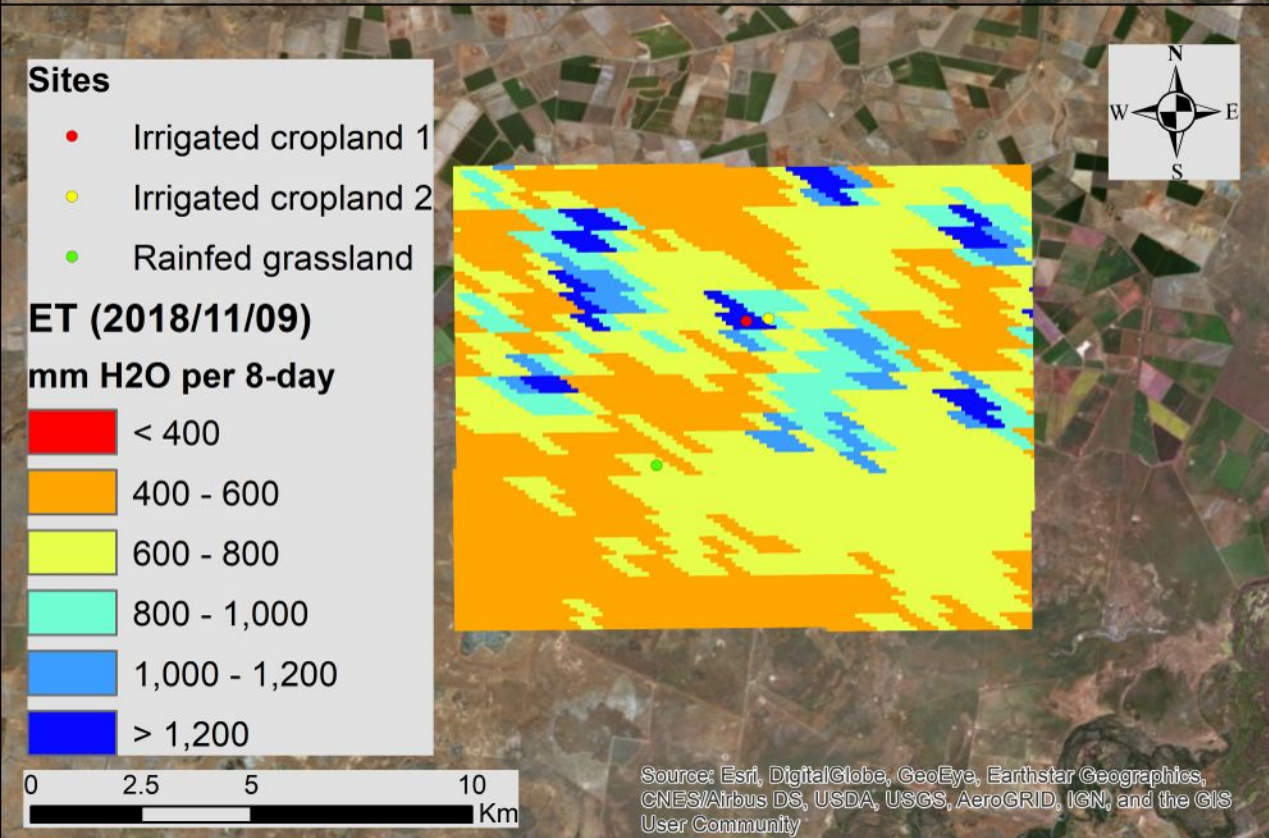
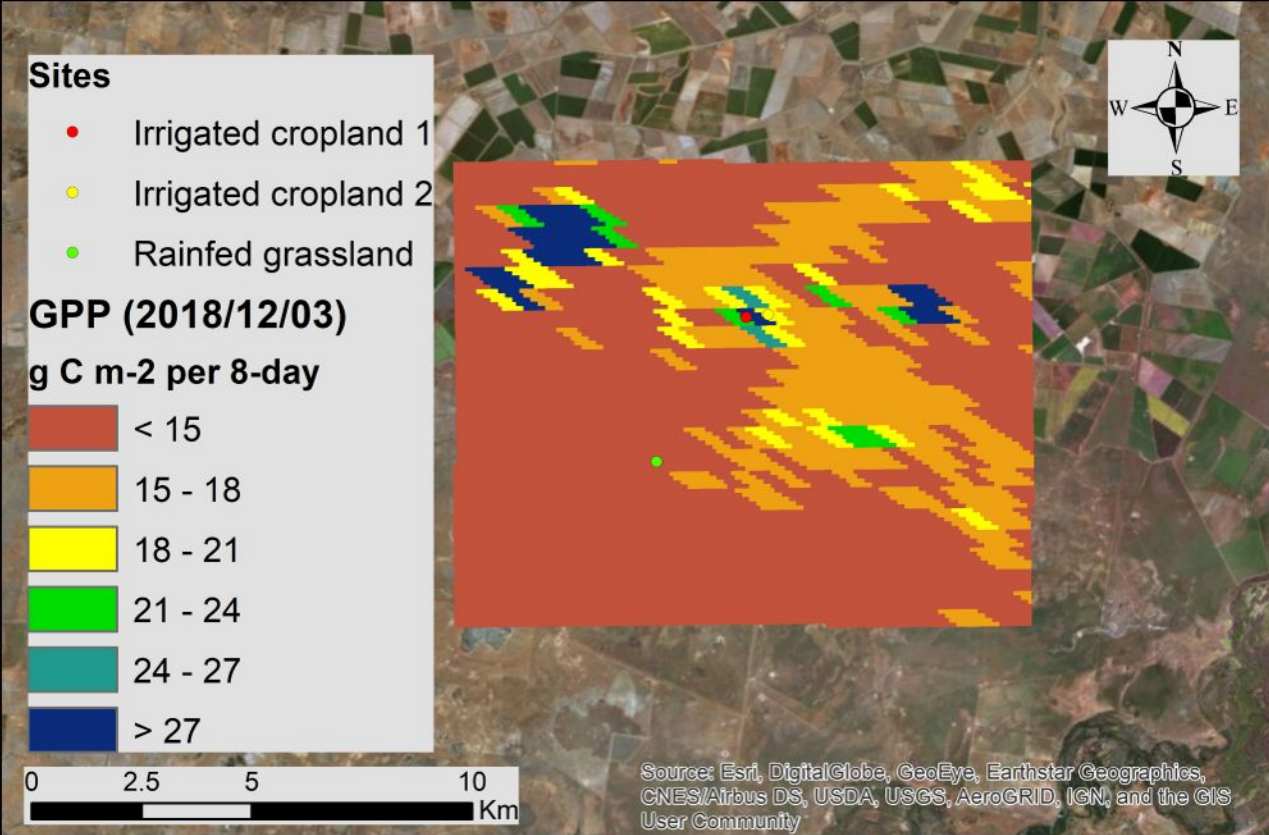
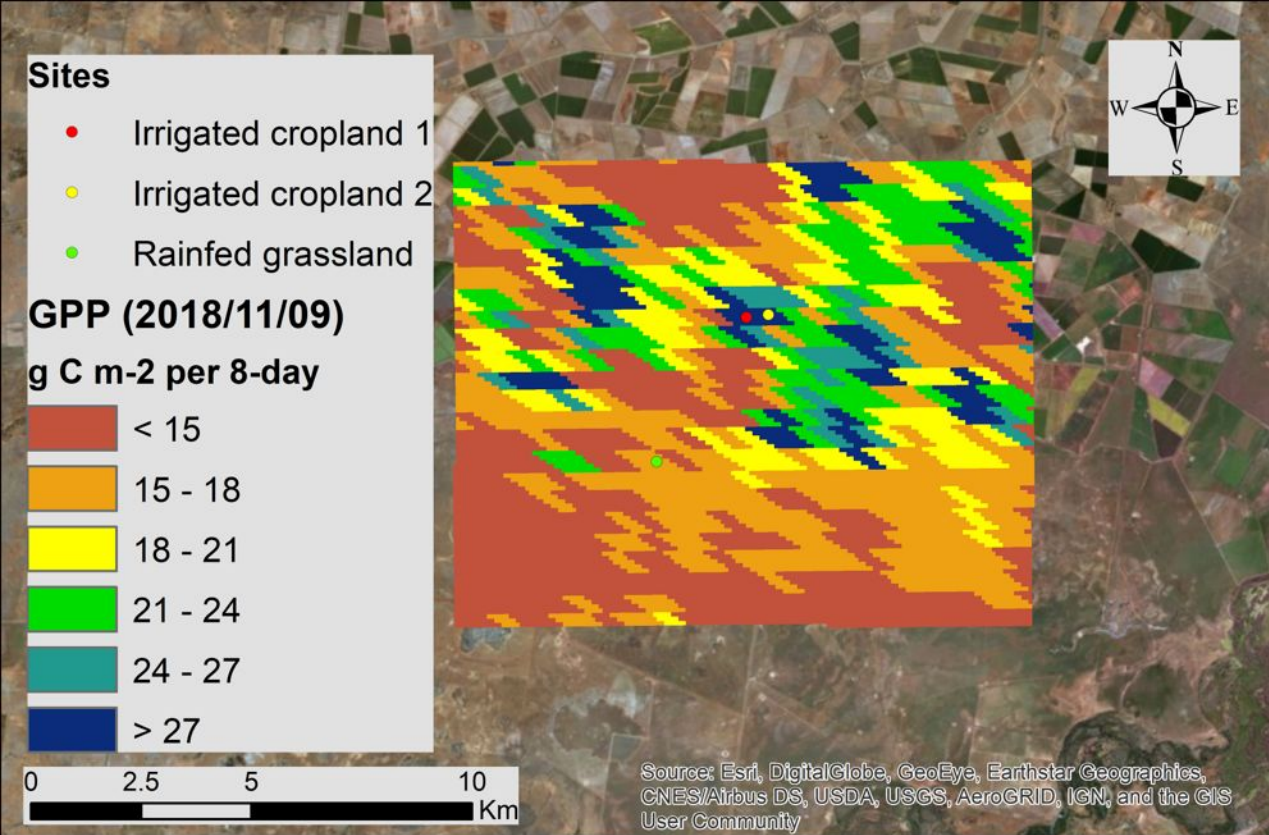


Figure7.

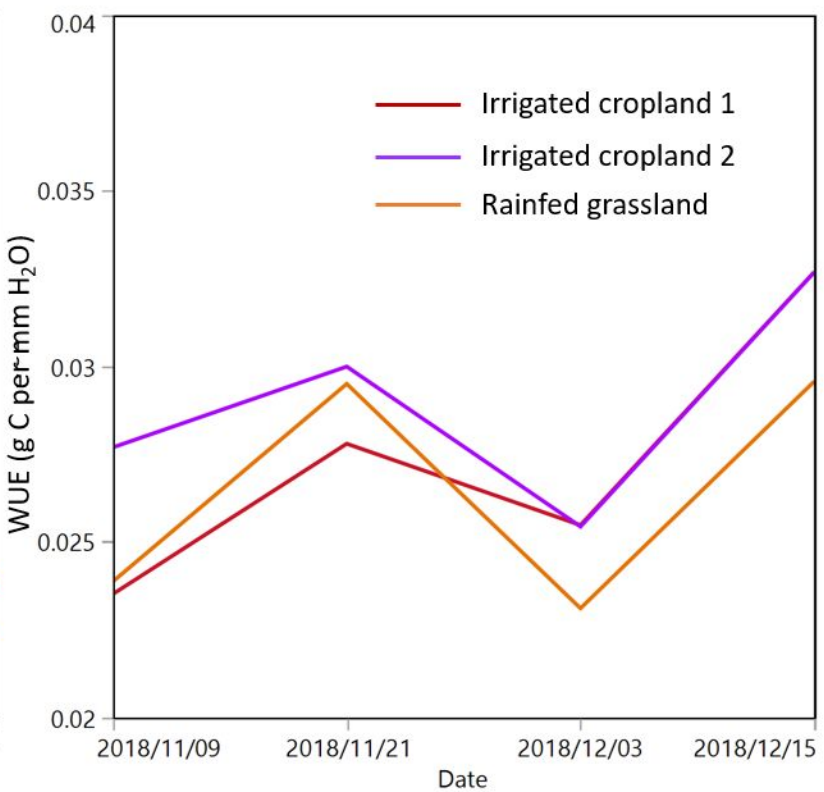
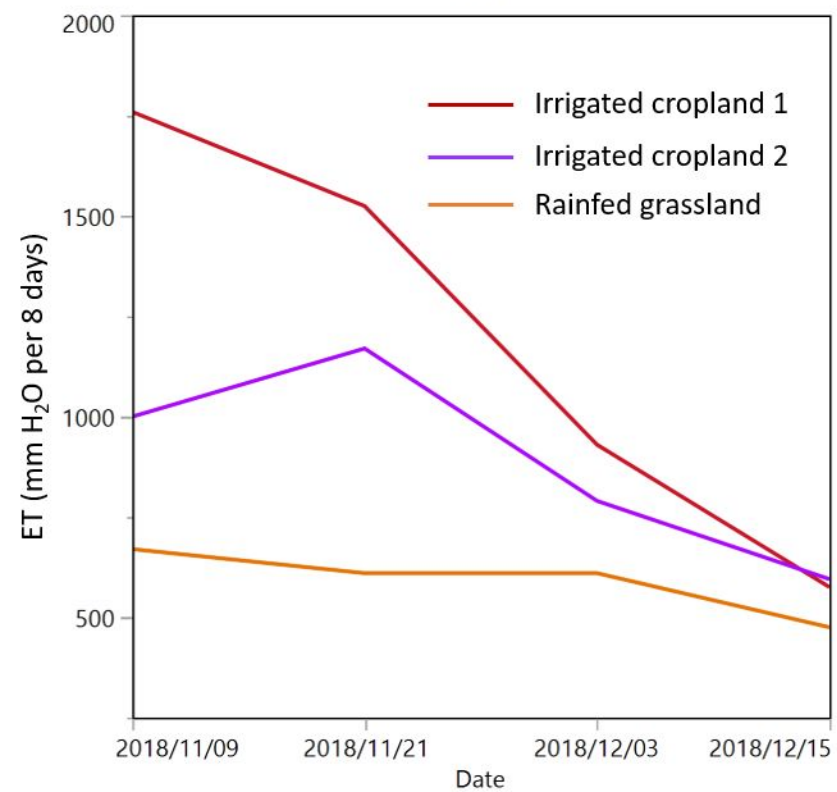
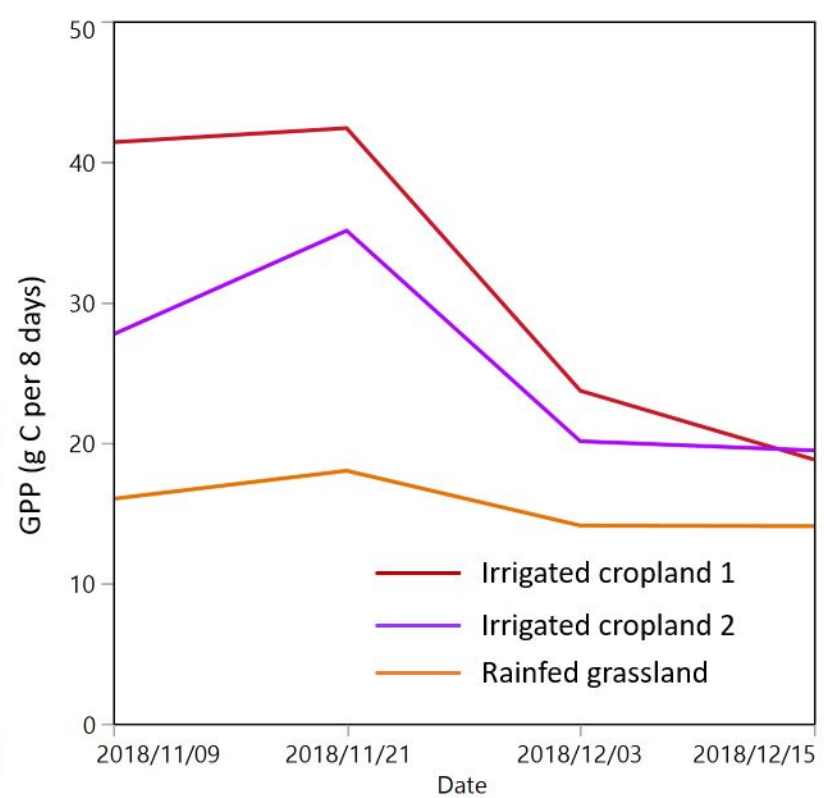
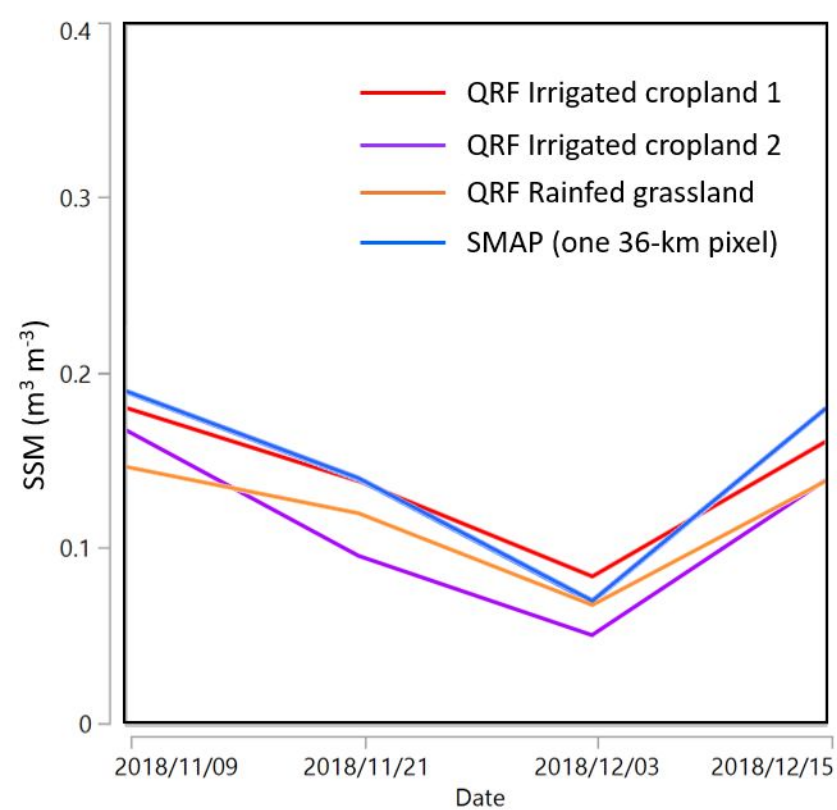
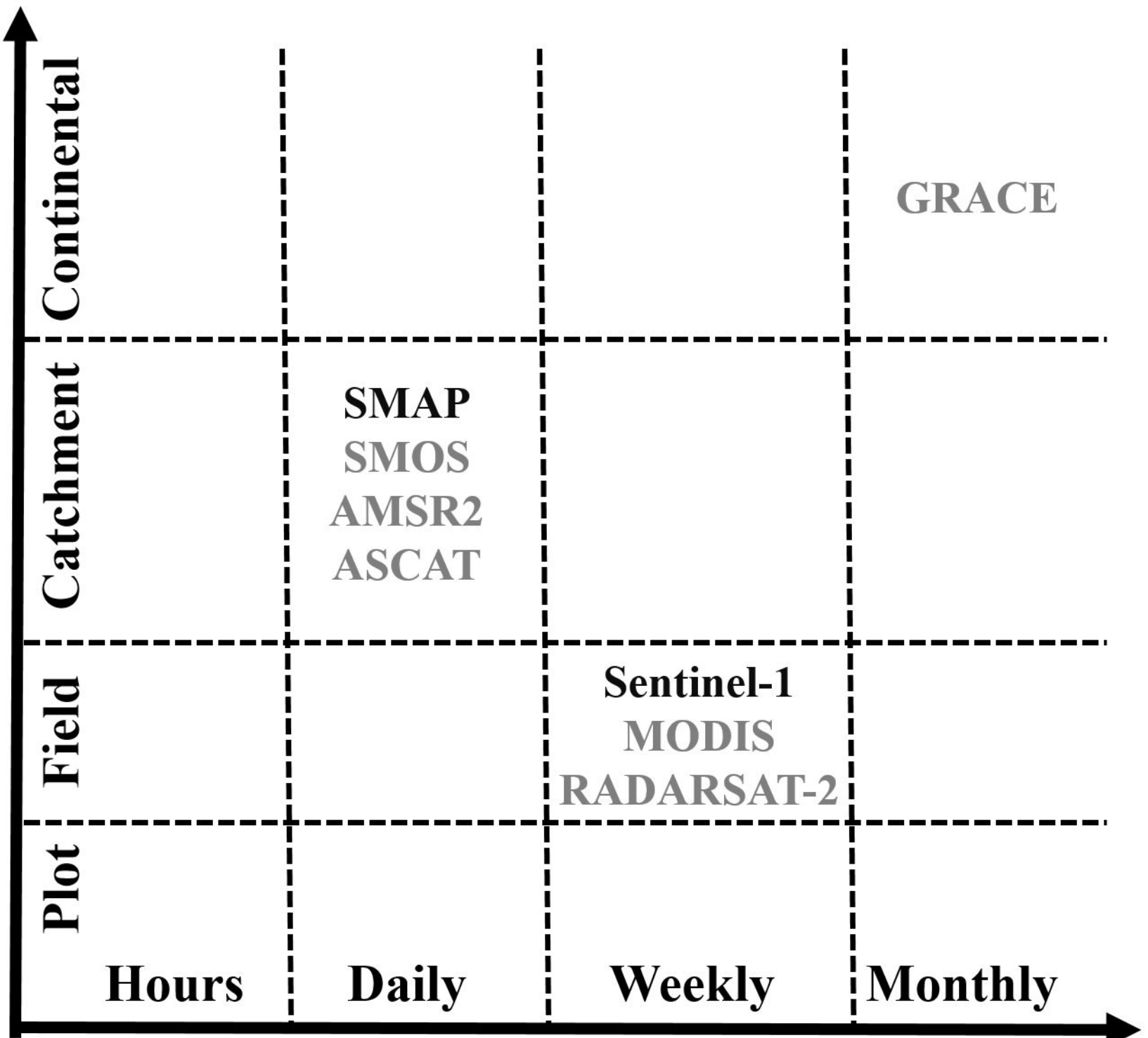


Figure 8.

Spatial resolution



Temporal resolution

Table 1 Remote sensing and land surface datasets used for modeling surface soil moisture (SSM) and interpretation.

Dataset	Measuring/Estimated variable	Spatial resolution	Measuring interval
NASA-SMAP (L3_SM_P)	Brightness temperature retrieved to surface soil moisture (0–0.05 m)	36 km	2-3 days
ESA-Sentinel-1	Time-varying backscatter, incident angle, and time-constant temporal statistics (min, mean, max, standard deviation)	5×20 m	6-12 days/N.A.
GMTED2010 digital elevation model	Slope, aspect, flow direction, topographic position index, topographic roughness index	500 m	N.A.
SoilGrids & Openlandmap	Clay, silt, sand contents, soil organic carbon content, bulk density, field capacity, permanent wilting point at depth 0–0.05 m	250 m	N.A.
MODIS (MCD12Q1.006)	Land cover types	500 m	N.A.
Station soil moisture monitoring networks	Soil water content at depth 0–0.05 m	N.A.	30-min

Table 2 Summary statistics of land cover types and surface soil moisture (SSM) at various regional-scale (HOBE, OZNET, REMEDHUS) and continental-scale (SCAN, USCRN) soil moisture monitoring networks for training and validation datasets.

Network	Country	No. Stations	Land cover	SSM (Training)					SSM (Validation)						
				No. stations	Min.	Mean	Median	Max	SD	No. stations	Min.	Mean	Median	Max	SD
HOBE	Denmark	24	Cropland (54%), Savanna (27%), Forest (18%)	18	0.03	0.19	0.18	0.49	0.08	6	0.00	0.18	0.17	0.38	0.09
OZNET	Australia	19	Cropland (52%), Grassland (48%)	14	0.00	0.14	0.14	0.40	0.09	5	0.00	0.15	0.15	0.40	0.08
REMEDHUS	Spain	12	Cropland (79%), Grassland (11%), Shrubland (10%)	8	0.00	0.10	0.09	0.33	0.07	4	0.05	0.20	0.18	0.45	0.09
SCAN	USA	147	Cropland (27%), Grassland (53%), Savanna (9%), Shrubland (5%), Forest (2%), Barren (4%)	109	0.00	0.16	0.13	0.58	0.12	38	0.00	0.18	0.16	0.55	0.12
USCRN	USA	76	Cropland (11%), Grassland (48%), Savanna (16%), Shrubland (13%), Forest (10%), Barren (3%)	56	0.00	0.16	0.14	0.55	0.11	20	0.00	0.21	0.19	0.61	0.11

Table 3 Comparison between measured surface soil moisture (SSM) with the predicted SSM from the quantile random forest (QRF) and SMAP based on the validation dataset. Note: r , Pearson’s correlation coefficient; ME, mean error; RMSE, root mean squared error; values inside the brackets are the minimum and maximum values calculated among all validation stations and values outside the brackets are overall values calculated by merging measurements from all the stations within a same land cover type.

Network	Land cover	Station names	No. Stations	No. measurements	QRF			SMAP		
					r	ME ($\text{m}^3 \text{m}^{-3}$)	RMSE ($\text{m}^3 \text{m}^{-3}$)	r	ME ($\text{m}^3 \text{m}^{-3}$)	RMSE ($\text{m}^3 \text{m}^{-3}$)
HOBE	Cropland	1.09, 3.04, 3.09	3	393	0.79 [0.65, 0.88]	0.01 [0.00, 0.01]	0.03 [0.03, 0.03]	0.74 [0.60, 0.84]	0.04 [0.03, 0.06]	0.06 [0.05, 0.07]
	Savanna	1.01, 3.06	2	431	0.62 [0.55, 0.58]	-0.01 [-0.08, 0.05]	0.08 [0.06, 0.11]	0.30 [0.54, 0.56]	0.04 [-0.05, 0.11]	0.11 [0.09, 0.12]
	Forest	1.04	1	135	0.58	0.52	0.58	0.52	0.58	0.52
OZNET	Cropland	Kyeamba_Mouth, Spring_Bank, Uri_Park, Wollumbi	4	159	0.60 [0.46, 0.86]	0.01 [-0.01, 0.05]	0.06 [0.04, 0.08]	0.63 [0.41, 0.83]	0.08 [0.06, 0.12]	0.13 [0.11, 0.14]
	Grassland	Cheverelis	1	29	0.88	0.90	0.88	0.90	0.88	0.90
REMEDHUS	Cropland	Canizal, Guarrati, Las_Bodegas	3	394	0.46 [0.29, 0.82]	-0.10 [-0.13, -0.03]	0.13 [0.05, 0.15]	0.42 [0.29, 0.81]	-0.10 [-0.13, -0.02]	0.13 [0.06, 0.16]
	Grassland	Las_Arenas	1	102	0.82	0.79	0.82	0.79	0.82	0.79
SCAN	Cropland	Abrams, Fort Reno #1, Molly Caren #1, North Issaquena, Perthshire, Princeton #1, Rock Springs Pa, Scott, Tidewater #1, Tunica, Uapb Dewitt, Uapb Point Remove, Uapb-Earle	13	817	0.66 [0.00, 0.79]	-0.01 [-0.07, 0.07]	0.08 [0.05, 0.11]	0.61 [0.04, 0.78]	0.02 [-0.05, 0.15]	0.10 [0.06, 0.15]
	Grassland	Alcalde, Bodie Hills, Crossroads, Jordan, Lindsay, Nephi, Stephenville, Torrington #1, Vermillion, Vernon, West Summit, Mandan #1, Price, Reese Center, Sheldon, Tule Valley, Violet, Walnut Gulch #1	18	1,878	0.60 [0.07, 0.89]	-0.01 [-0.09, 0.07]	0.07 [0.04, 0.11]	0.64 [0.07, 0.87]	-0.01 [-0.08, 0.07]	0.07 [0.03, 0.10]
	Savanna	Pee Dee, Powell Gardens, Morris Farms	3	199	0.79 [0.54, 0.71]	-0.03 [-0.08, 0.00]	0.07 [0.04, 0.10]	0.41 [0.57, 0.70]	0.06 [-0.04, 0.14]	0.11 [0.06, 0.15]
	Shrubland	Spooky	1	126	0.16	0.08	0.08	0.19	0.05	0.05
	Forest	Reynolds_Homestead	1	45	0.60	0.02	0.08	0.56	0.14	0.15
	Barren	Death Valley Jct., Lovelock NNR	2	222	0.79 [0.26, 0.70]	0.04 [0.04, 0.05]	0.05 [0.05, 0.06]	0.78 [0.22, 0.67]	0.05 [0.05, 0.05]	0.06 [0.05, 0.06]
USCRN	Cropland	IA_Des_Moines_17_E, KY_Versailles_3_NNW,	4	364	0.68	-0.03	0.07	0.57	-0.02	0.08

		NE_Lincoln_8_ENE, MO_Joplin_24_N			[0.62, 0.82]	[-0.07, 0.00]	[0.05, 0.09]	[0.63, 0.77]	[-0.09, 0.05]	[0.06, 0.11]
	Grassland	MT_Dillon_18_WSW, MT_Wolf_Point_34_NE, NC_Ashville_13_S, NE_Whitman_5_ENE, OK_Stillwater_2_W, OR_John_Day_35_WNW, SD_Aberdeen_35_WNW, SD_Pierre_24_S, TX_Muleshoe_19_S, MT_Lewistown_42_WSW, OR_Riley_10_WSW	11	1,022	0.65 [0.48, 0.91]	-0.01 [-0.08, 0.07]	0.07 [0.03, 0.10]	0.70 [0.47, 0.92]	-0.01 [-0.09, 0.06]	0.07 [0.03, 0.10]
	Savanna	IN_Bedford_5_WNW, MN_Goodridge_12_NNW	2	149	0.50 [0.45, 0.83]	-0.07 [-0.14, -0.04]	0.12 [0.08, 0.19]	0.67 [0.50, 0.81]	-0.03 [-0.07, -0.01]	0.08 [0.06, 0.13]
	Shrubland	CA_Fallbrook_5_NE	1	163	0.68	-0.04	0.05	0.87	-0.04	0.04
	Forest	CO_Boulder_14_W	1	152	0.58	-0.03	0.07	0.61	0.00	0.06
	Barren	ID_Arco_17_SW	1	39	0.85	0.05	0.07	0.87	0.03	0.05
Overall	Cropland	-	27	2,127	0.73 [0.00, 0.88]	-0.02 [-0.13, 0.07]	0.08 [0.03, 0.15]	0.64 [0.04, 0.84]	0.00 [-0.13, 0.15]	0.10 [0.05, 0.16]
	Grassland	-	31	3,031	0.63 [0.07, 0.91]	-0.01 [-0.09, 0.07]	0.07 [0.03, 0.11]	0.67 [0.07, 0.92]	-0.01 [-0.09, 0.07]	0.07 [0.03, 0.10]
	Savanna	-	7	779	0.73 [0.45, 0.83]	-0.02 [-0.14, 0.05]	0.09 [0.04, 0.19]	0.54 [0.50, 0.81]	0.03 [-0.07, 0.14]	0.11 [0.06, 0.15]
	Shrubland	-	2	289	0.22 [0.16, 0.68]	0.01 [-0.04, 0.08]	0.07 [0.05, 0.08]	0.78 [0.19, 0.87]	0.00 [-0.04, 0.05]	0.05 [0.04, 0.05]
	Forest	-	3	332	0.58 [0.58, 0.60]	-0.05 [-0.11, 0.02]	0.09 [0.07, 0.11]	0.63 [0.52, 0.61]	0.01 [-0.03, 0.14]	0.08 [0.06, 0.15]
	Barren	-	3	261	0.77 [0.26, 0.85]	0.04 [0.04, 0.05]	0.05 [0.05, 0.07]	0.77 [0.22, 0.87]	0.04 [0.03, 0.05]	0.06 [0.05, 0.06]